

## APPENDIX A

### Additional Experiments

#### Methods

#### Strains

Strains used in this work were as cited in [1]. Additional strains used include:

XA6226 *mrg-1(qa6200)/qC1 dpy-19(e1259) glp-1(q339)[qls26]* III (gift from Kentaro Nabeshima)

RB2083 (TFIIS) *T24H10.1(ok2749)* II (obtained from the CGC)

#### RNA interference

RNA interference was conducted as described in [1].

#### Antibodies

Antibodies used include those employed in [1]. Other antibodies used include: anti-MRG-1 (gift from Kentaro Nabeshima); anti-H3K36me2 (Abcam, 1:200); anti-H3K36me3 (Abcam, 1:200); anti-DPY-21 (Novus, 1:200); s9.6 (gift from Bradley Cairns); RNA Pol II 4H8 (Abcam, 1:250); anti-SIR-2.1 (Abcam, 1:100).

#### Western blotting

Western blotting (Figure A1.1) was conducted as in [1], using L4 worms instead of embryos in Figure A1.1B.

### **Immunoprecipitation**

Immunoprecipitation (Figure A1.1) was conducted as in [2].

### **Immunofluorescence (A1.2, 1.3, 1.5, 1.6, 1.7, 1.8, 1.13, 1.16, 1.17, 1.22, 1.23, 1.28)**

Immunofluorescence analysis, except in Figure A1.20, was conducted as in [1].

### **FISH (A1.21)**

Fluorescent *in situ* hybridization (FISH) analysis was conducted as in [1], using custom (cDNA) primers designed against exons 1-3 of *dpy-27*, the N-terminus to the middle of exon 6 of *dpy-21*, or exon 6 of *dpy-21*.

### **ImmunoFISH (A1.20, A1.28)**

ImmunoFISH analysis was conducted as in [1] for Figure A1.20; for Figure A1.28, IF was followed by ethanol washes, wash in 4% PFA in PBS for 10 mins., then followed by FISH.

### **Immunofluorescence with direct labeling**

Immunofluorescence with direct labeling (Figure A1.9) was conducted as in [1], with the following modifications. Primary antibodies (DPY-27, 1:200) were directly labeled using the Invitrogen Zenon® Tricolor Rabbit IgG Labeling Kit (Invitrogen Z-25360), following the manufacturer's protocol. Exposure times were as follows: CY3 – 150 ms, FITC – 160 ms, CY5 – 3500 ms.

### **WIG correlations and SitePro meta-analysis**

WIG file correlations and SitePro meta-analysis (Figs. A1.24-A1.27) was conducted as described in the Chapter 3 Methods, except that short capped RNA metagenes (Figures A1.29-A1.32) were mapped at 22bp resolution.

### **Public Datasets**

Downloaded from <http://www.modencode.org> or NCBI GEO

Format: Dataset ID, Description (Stage), Array (if applicable)

43; HTZ-1 ME; direct wiggle file download

### **Metagene analysis and wiggle file creation**

Metagene analysis (Fig. A1.27) was conducted as described in the Chapter 3 Methods, with the following additions. In order to construct a working HTZ-1 ME wiggle file, the replicate wiggle files were downloaded from [modencode.org](http://modencode.org) (modENCODE\_43), uploaded to Galaxy ([http://bifx-core.bio.ed.ac.uk:8080/root?tool\\_id=int2wig](http://bifx-core.bio.ed.ac.uk:8080/root?tool_id=int2wig)), converted to interval format (“Wiggle-to-Interval” function), and combined by maximum value (“Wiggle Merge” function). The merged wiggle file was converted to a useful wiggle format using `BedToWig.sh` (<http://genomewiki.ucsc.edu/index.php/File:BedToWig.sh>) on the University of Michigan servers. Resulting files were manually transformed in Microsoft Excel 2007 and assembled in Notepad++ ([notepad-plus-plus.org/](http://notepad-plus-plus.org/)) to make the final, usable wiggle file uploaded to Cistrome.

### **Genetics Teaching Data & Statistics**

Genetics teaching data (Figure A1.10) were obtained from a joint request with Lisa Sramkowski (Witkopp Lab) to the Registrar’s Office and from Dr. Györgyi Csankovszki’s personal computer with permission. Data were de-identified by the University of Michigan’s Registrar’s Office following reorganization into a standardized, concise format. Boxplots were constructed using Minitab 11 Student Edition; topics analysis was conducted in Microsoft Excel 2007. ANOVA and Tukey tests for these sections were conducted in Minitab 16. Mixed Linear Model analysis was conducted in Stata 11.

### **Chromatin Immunoprecipitation**

Chromatin immunoprecipitation (Figure A1.11) was conducted as described in [3]. Pull-down DNA was then used for downstream PCR analysis.

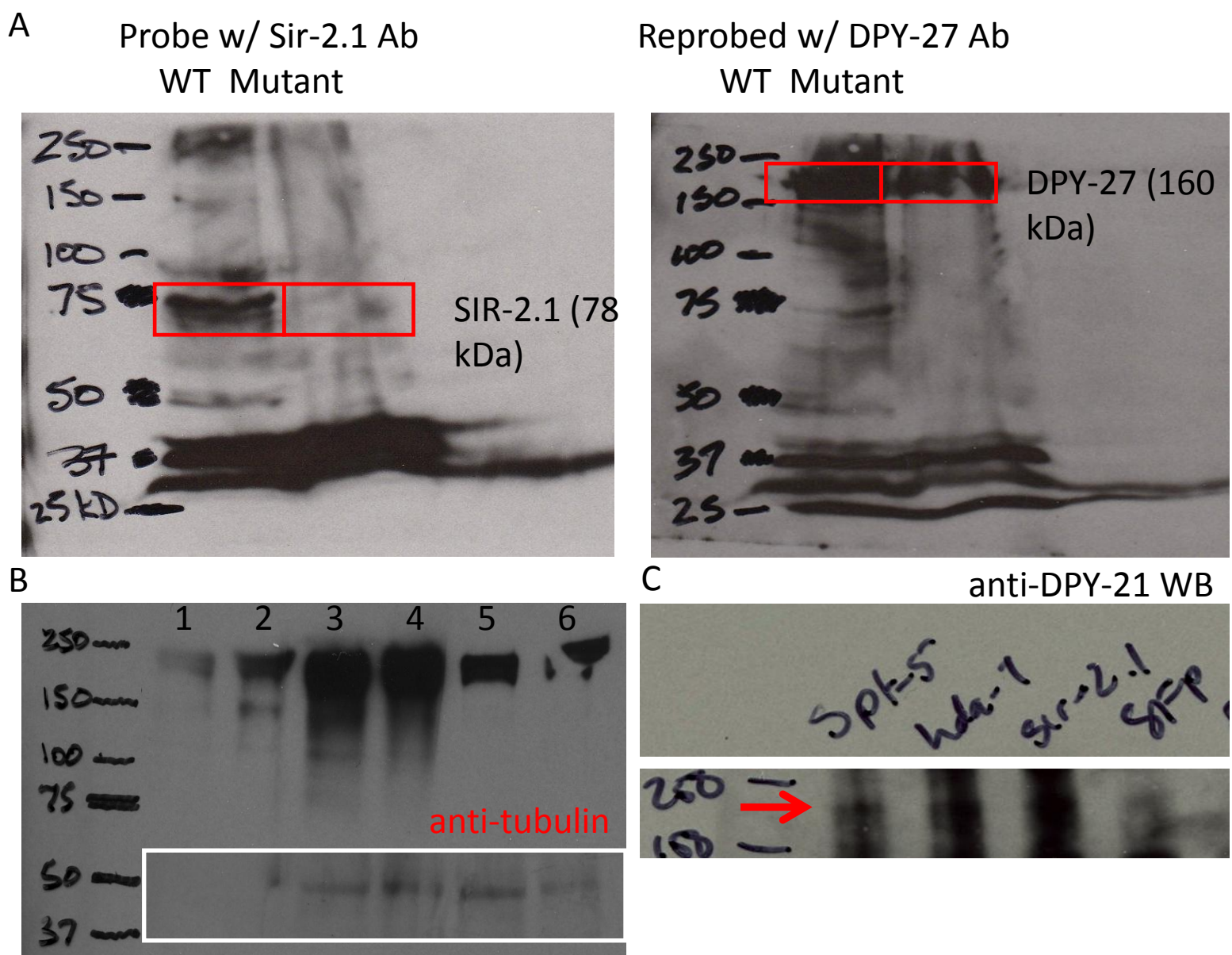


**Figure A1.1. Western blots investigating SIR-2.1 antibody specificity, RNA Pol II state changes between WT and *dpy-21(e428)*, and interactions with DPY-21 following IP of chromatin and RNA Pol II regulators.** A) (left) anti-SIR-2.1 recognizes a 78 kDa band (which is the expected size) in WT, but not *sir-2.1(ok434)* whole L4 worm extract; additional bands of unknown origin are also recognized. The blot was re-probed (right) with anti-DPY-27 to demonstrate equivalent sample loading. The band size expected in the mutant (37 kDa) was not visible due to antibody light chain interference. B) RNA Pol II state comparison between WT and *dpy-21(e428)* L4 whole worm extract as follows: Lanes 1 & 2 - P-Ser5 (Abcam ab5131; lot 898958), Lanes 3 & 4 - P-Ser2 (Abcam ab5095), Lanes 5 & 6 - hypo-phosphorylated RNA Pol II (4H8; Abcam ab5408); odd lanes - WT extract, even lanes - *dpy-21(e428)* extract. Results show that despite a loss in P-Ser5 signal in *dpy-21(e428)* by IF (Figure 4.4A), levels of P-Ser5 are similar, if not higher in this mutant by Western blot. P-Ser2 and 4H8 (which recognizes RNA Pol II not phosphorylated at Ser2 [4-6]) are similar between samples. Anti-tubulin is shown as a loading control. C) Performed by Martha Snyder. Following immunoprecipitation using antibodies against SPT-5, HDA-1, SIR-2.1, or GFP in WT embryo extracts, Western analysis was used to look for interactions with DPY-21. Results show faint bands of the expected size in all lanes except GFP control, indicating weak associations between DPY-21 and this regulatory machinery.

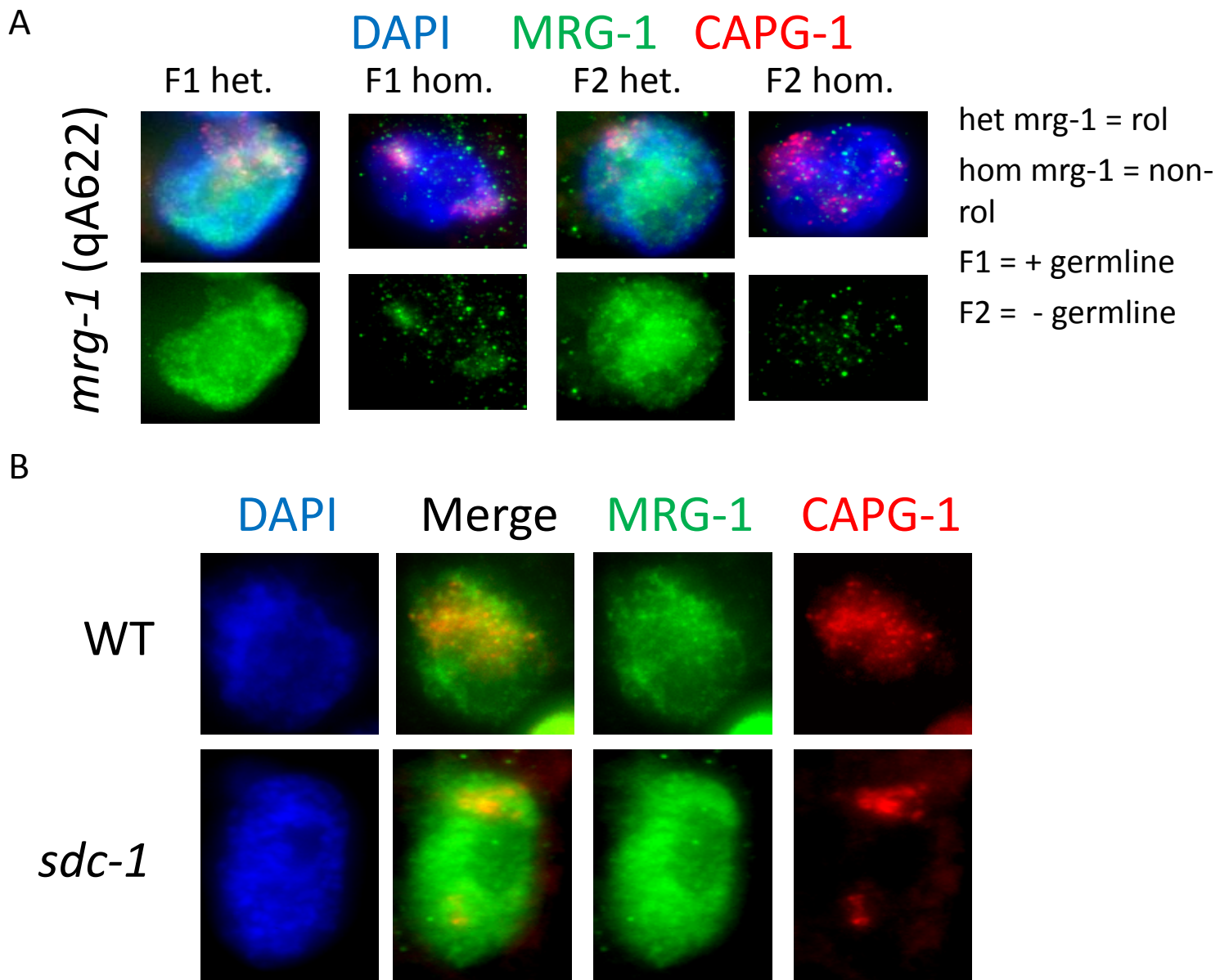


**Figure A1.2. MRG-1 localization.** Immunofluorescence using anti-MRG-1 (gift from Kentaro Nabeshima) and anti-CAPG-1 in *mrg-1*(qA622) (A) or WT and *sdc-1*(y415) (B). DAPI (DNA) is shown in blue. A) Homozygous progeny show very little signal, as expected, while heterozygotes show robust staining - both results are as expected, suggesting good antibody specificity. B) MRG-1 localization, indicative of simultaneous TIP60 complex and RPD3 complex localization, is similar in WT and *sdc-1*(y415).

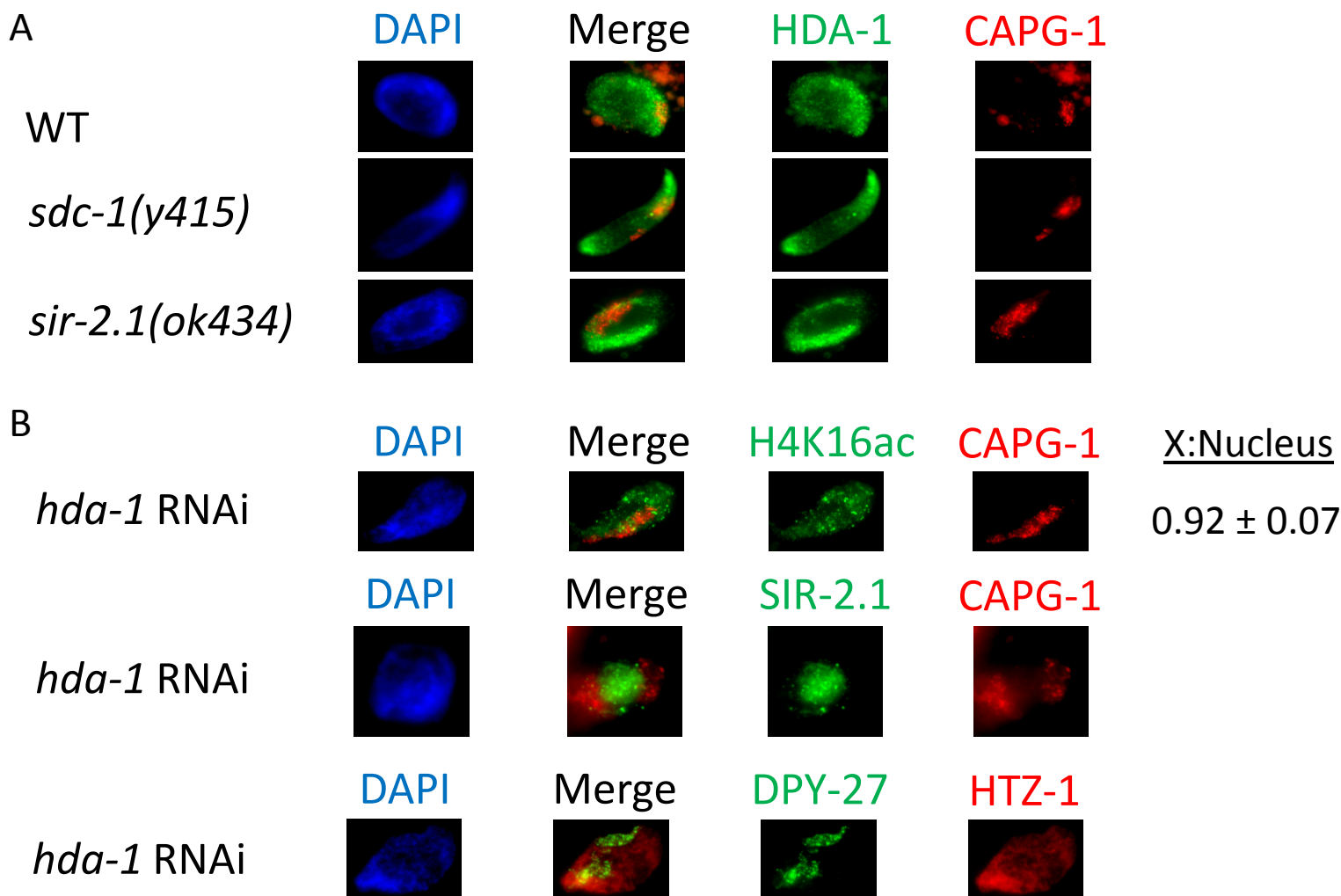


**Figure A1.3. HDA-1 localization and *hda-1 RNAi* effects on chromatin and markers of dosage compensation function.** Immunofluorescence analysis of anti-HDA-1 in WT, *sdc-1(y415)*, or *sir-2.1(ok434)* hermaphrodites (A), or anti-H4K16ac, anti-SIR-2.1, or anti-HTZ-1 costained with either anti-CAPG-1 or anti-DPY-27 in WT worms treated with *hda-1 RNAi* (B). DAPI (DNA) is shown in blue. A) Anti-HDA-1 and anti-CAPG-1 staining in WT, *sdc-1(y415)*, and *dpy-21(e428)* hermaphrodite gut nuclei. Staining is fairly uniform in WT, but becomes more and more concentrated to a region that is not X with loss of dosage compensation function. B) Anti-H4K16ac, Anti-SIR-2.1, or Anti-HTZ-1 costained with anti-DCC antibodies in WT hermaphrodite gut nuclei following treatment with *hda-1 RNAi*. Results show that H4K16ac depletion seen on X in WT worms (see Chapter 2) is partially lost with *hda-1* knockdown. Also, SIR-2.1 localization to DNA is lost (becoming nucleolar instead); HTZ-1 levels appear similar to WT.

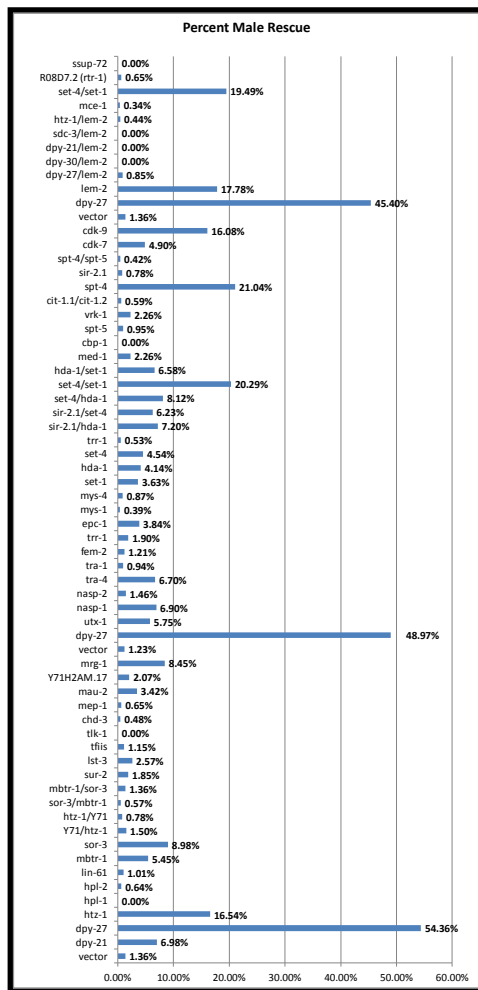


**Figure A1.4. Results of modified *xol-1* suppression assay to determine contributions to dosage compensation function.** This assay was conducted as described in [1]. Results were grouped based on common functional pathways. *ssup-72*, *R08D7.2*, and *mce-1*: capping enzyme and RNA Pol II CTD Ser5 phosphatases. No rescue beyond vector controls was seen. *vector*, *dpy-27*, *lem-2*, and *lem-2* combinations. *lem-2* RNAi leads to significant male rescue, but this effect is lost when combined with DCC complex member RNAi. This is odd, since DCC member RNAi (e.g. *dpy-27*), rescues males on its own. This loss of rescue effect could indicate that *lem-2* functions as part of an “autosomal downregulation” mechanism, an alternative to the hypothesized X upregulation mechanism previously hypothesized to play a role in global gene expression equalization between X and A within an individual. *cdk-9* through *trr-1*, *tftis*, and *tkl-1*: chromatin and RNA Pol II regulators. Results show that several factors contribute to dosage compensation function, either by acting on the DCC, RNA Pol II, or chromatin, including: *cdk-9*, *spt-4*, *hda-1 set-1*, *set-4 set-1*, *set-4 hda-1*, *sir-2.1 set-4*, and *sir-2.1 hda-1*. *tra-1* through *vector*: regulators of sex determination. Many of the maleness repressors, but not *nasp-2*, behave similarly to *DPY-21*, further indicating that *DPY-21* action in sex determination and dosage compensation may involve these proteins. *mrg-1*, a component of histone acetylation and deacetylation complexes, showed significant male rescue. *Y71H2AM.17* through *vector*: H4K20me1 binding domain-containing proteins, SWI/SNF components, and HP1 homologs. Only *mbtr-1* showed significant male rescue.



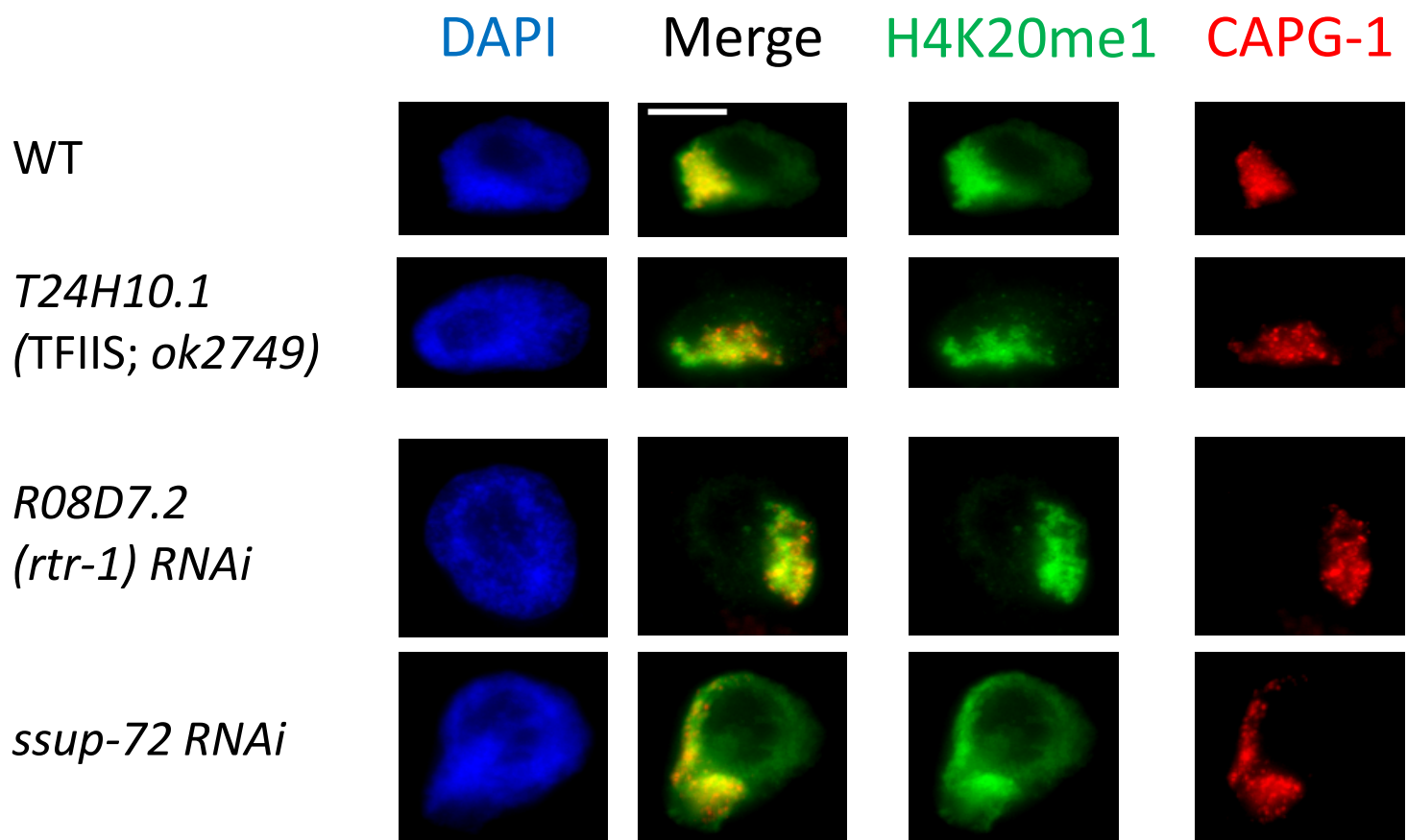


**Figure A1.5. TFIIS and RNA Pol II CTD Ser5 phosphatases are not essential to dosage compensation-directed chromatin repression.** Anti-H4K20me1 costained with anti-CAPG-1 in WT, *T24H10.1(ok2749)*, *R08D7.2* RNAi, or *ssup-72* RNAi. DAPI (DNA) is shown in blue. Results show H4K20me1 enrichment on X similar to WT in all cases, except a slight loss of enrichment after *ssup-72* RNAi, consistent with the role of the associated protein's in transcription elongation fidelity.

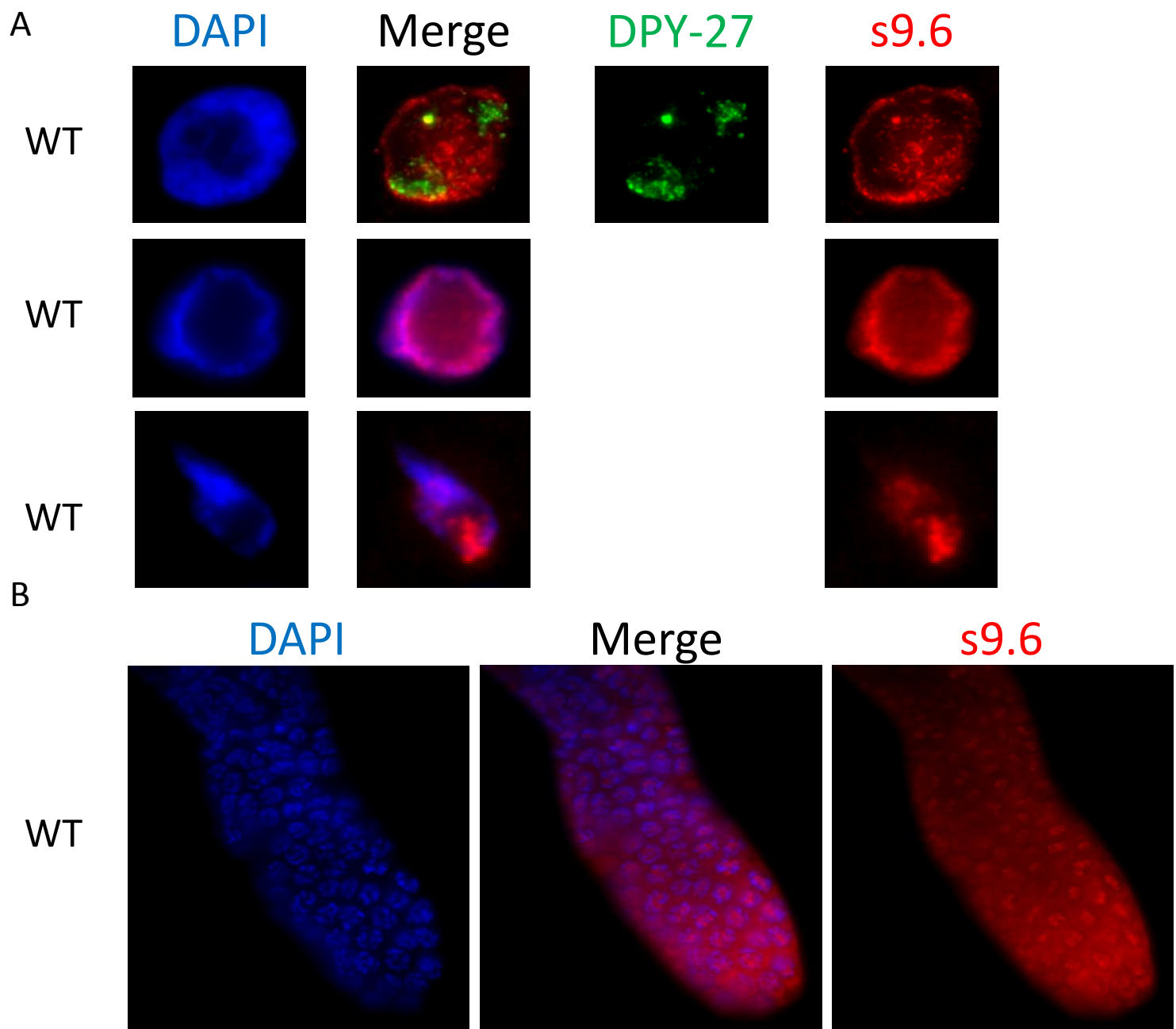


**Figure A1.6. Localization of staining from RNA-DNA hybrid antibody s9.6 in *C. elegans*.** Shown is staining from various somatic nuclei (A), or the mitotic germline (B) with s9.6 and anti-DPY-27 antibodies following the protocol described in [7]. DAPI (DNA) is shown in blue. Germline results in (B) suggest that this antibody, unlike in other systems, this antibody recognizes RNA duplexes in *C. elegans*, and if there is also RNA-DNA hybrid recognition, it is not enriched on the X chromosomes in somatic cells (A).

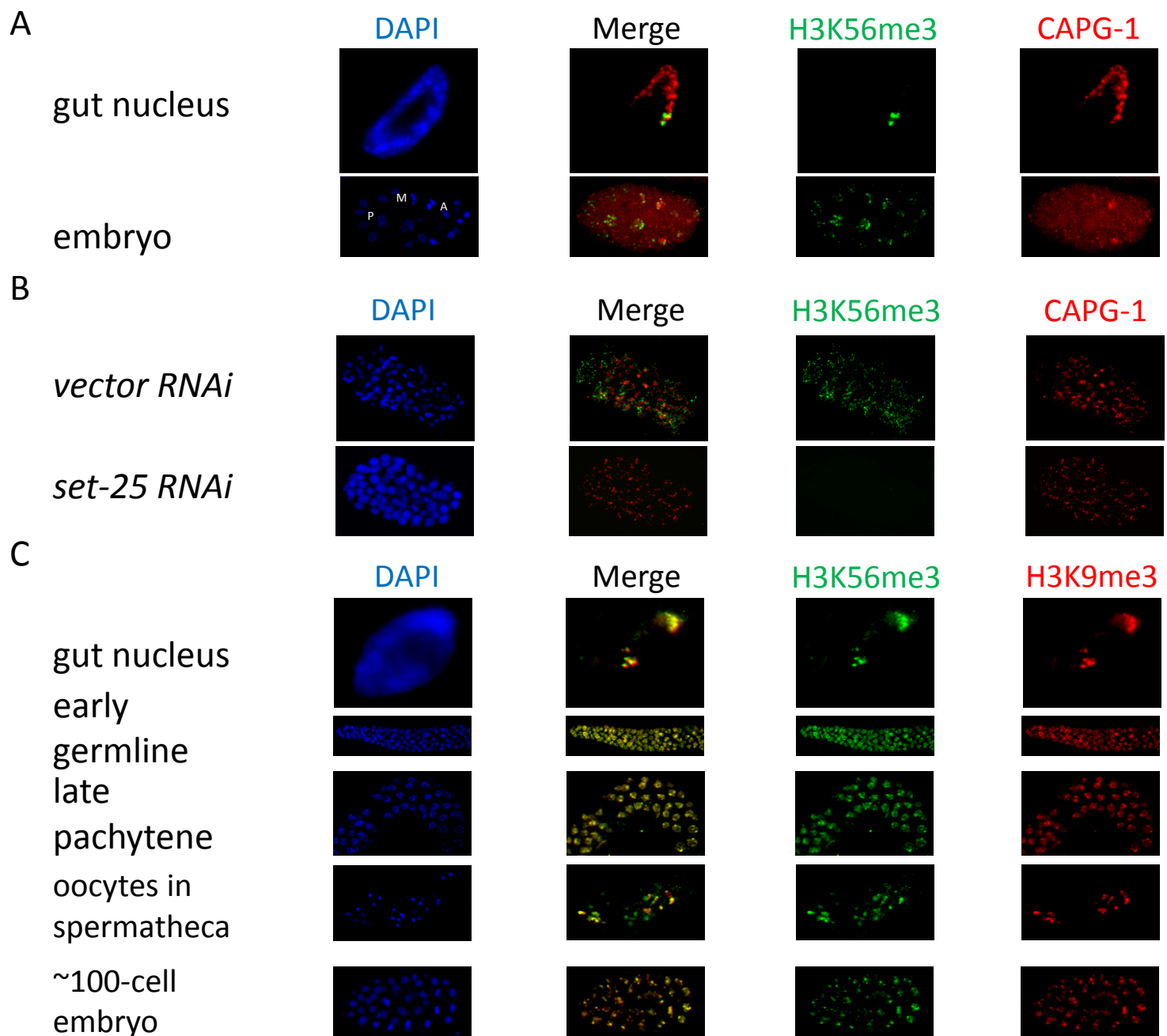


**Figure A1.7. H3K56me3 is conserved in *Caenorhabditis elegans*.** Immunofluorescence in adult *C. elegans* hermaphrodites. In all images, anti-H3K56me3 is shown in green, anti-H3K9me3 or anti-CAPG-1 in red, and DAPI (DNA) in blue. Scale bar = 5 microns. A) H3K56me3 relation to the Condensin component CAPG-1. Several punctate foci are present in somatic cells, near one end of the X chromosomes, marked by the DCC (CAPG-1). Further, H3K56me3 foci are present on and around the chromosomes during mitosis in embryos. B) SET-25, a conserved H3K9 methyltransferase, is responsible for H3K56me3 staining. Compared to robust signal seen in 100–200-cell embryos seen with vector RNAi treatment, *set-25* RNAi leads to a near complete loss of H3K56me3. This effect was not seen with several other methyltransferases tested (see below; data not shown). C) H3K56me3 colocalizes with H3K9me3, a mark of chromatin repression. H3K56me3 and H3K9me3 staining colocalize in gut nuclei (soma), the mitotic germline through transition zone, throughout pachytene, in oocytes, and in the developing embryo. However, H3K56me3, but not H3K9me3, staining was present in sperm.

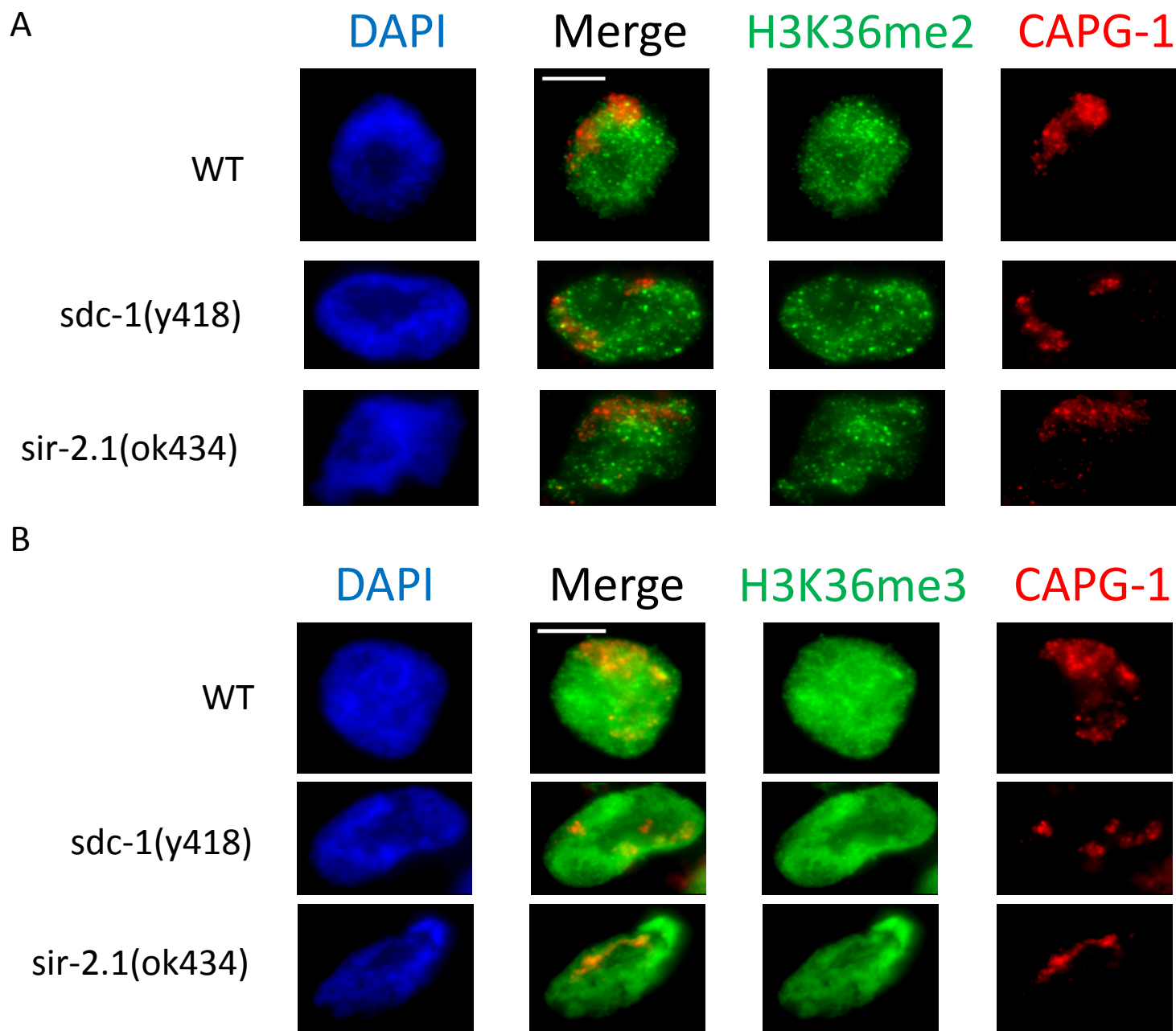


**Figure A1.8. H3K36me2 and H3K36me3 localization across the genome.** Shown are WT, *sdc-1(y415)*, or *dpy-21(e428)* hermaphrodite gut nuclei stained with anti-CAPG-1 and anti-H3K36me2 (A) or H3K36me3 (B). DAPI (DNA) is shown in blue. A) Similar to that seen by other groups in the germline, H3K36me2 is depleted on X in somatic nuclei of L4/young adult worms. B) H3K36me3 staining is similar across the nucleus in all three strains.

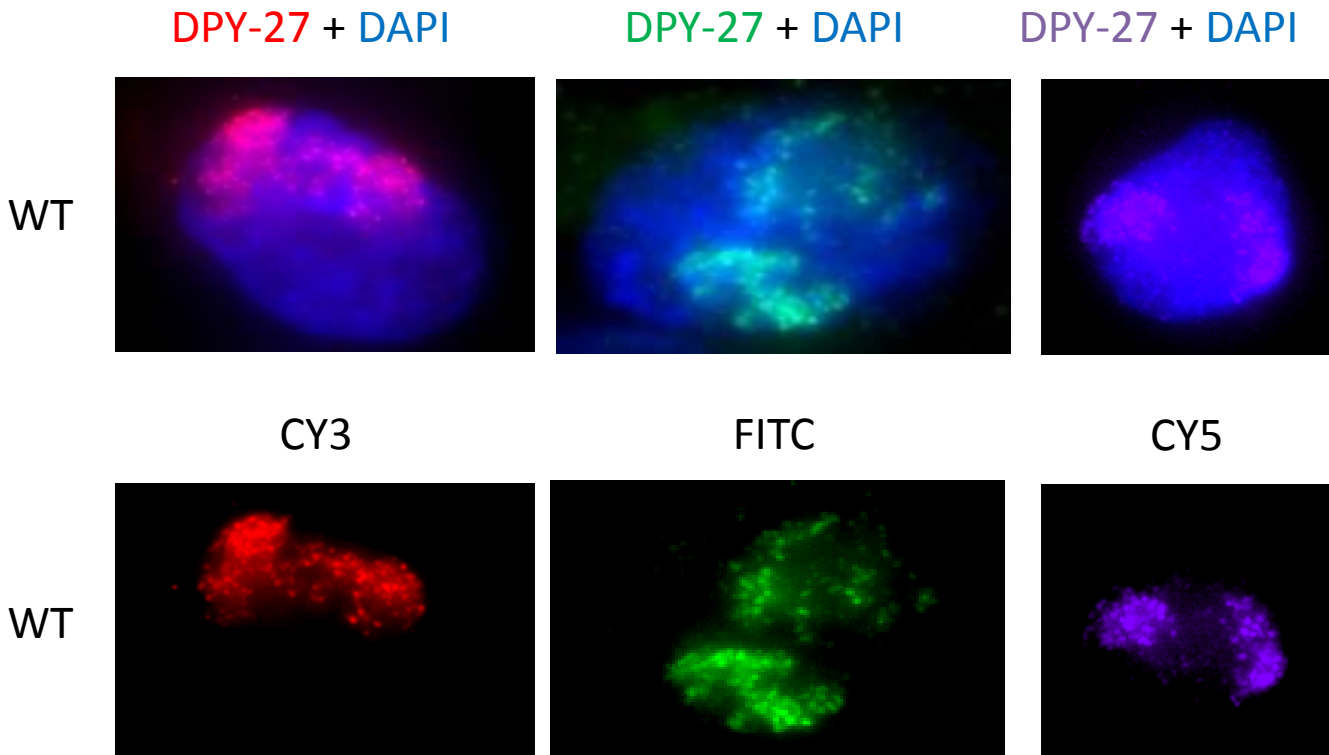


**Figure A1.9. Direct labeling kit enables potential use of multiple rabbit antibodies for single slide costaining.** Shown are WT hermaphrodite gut nuclei stained singly with anti-DPY-27 directly labeled using the Invitrogen Zenon Labeling kit. DAPI (DNA) is shown in blue. Results show that each fluorescent label works with this antibody. Exposure times varied greatly, and twice as much primary antibody is required than for traditional staining.

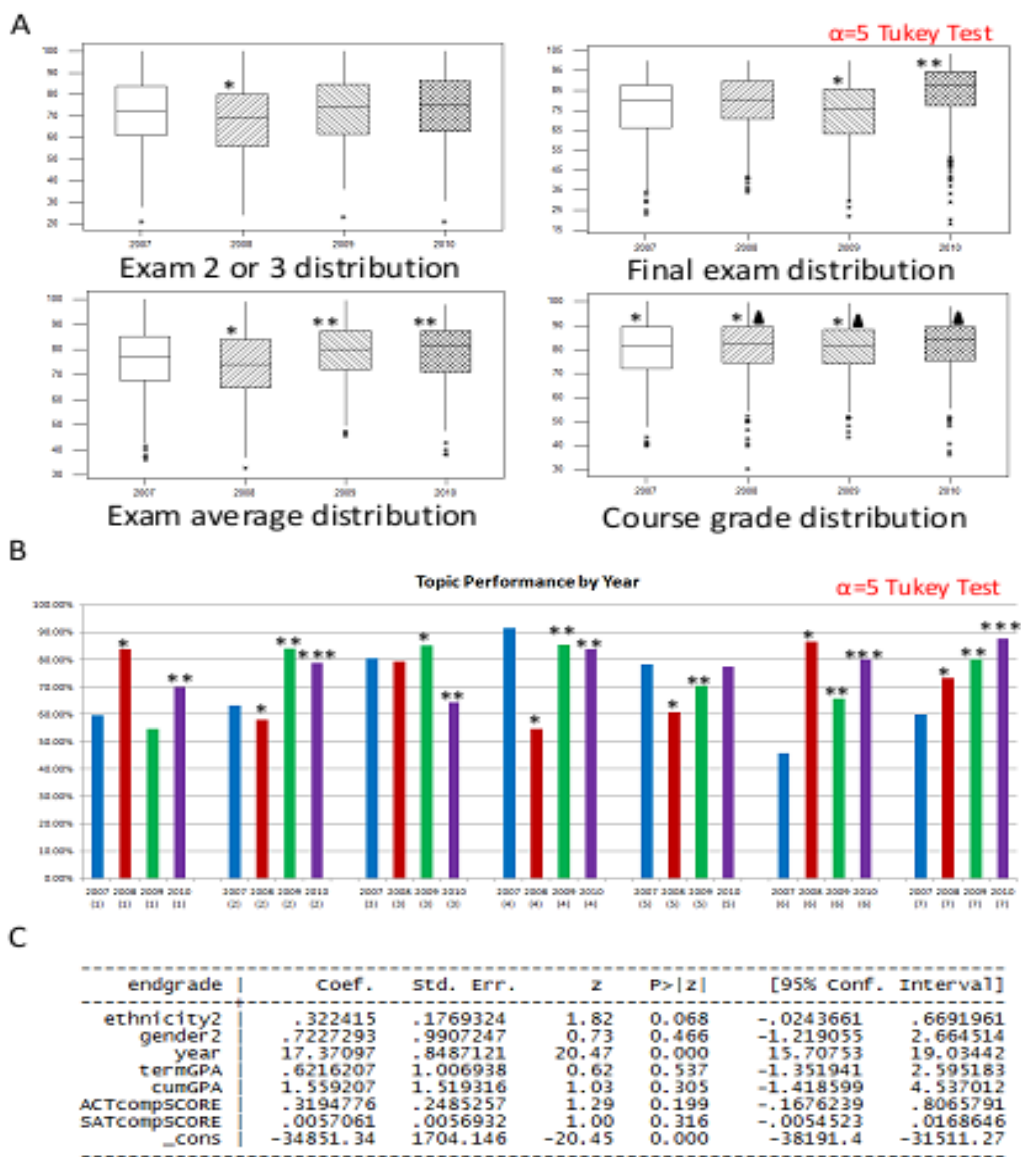


**Figure 1.10. Summary of analysis of teaching data from undergraduate Genetics.** A) Summary boxplots of exam scores, exam score averages, or course grades between 2007 and 2010 in undergraduate Genetics (BIO-305 at the University of Michigan). Significance categories are designated by the number of asterisks, with reference to the 2007 scores. In 2007, neither online quizzes or in-class use of student response devices were included in the course. 2008 included clickers, and 2009 included online quizzes. 2010 Genetics included both tools. B) Summary of topics analysis across years. Exam question categories were as follows: 1) 5' vs. 3', strand terms, 2) Northern, Southern, and Western blotting, 3) transcription machinery, DNA regulatory elements, 4) DNA to amino acid conversions, anticodons, 5) PCR, restriction digests, cloning, sequence coverage, 6) types of mutations, gain/loss-of-function mutations, complementation testing, and 7) cell cycle, meiosis/mitosis, and DNA replication. Results suggest that performance varies with exam difficulty, not consistent with the teaching methodologies employed each year (A). C) Mixed linear model analysis finds no demographic factors, beyond year in which student took the course, which contribute to exam grades. Factors tested include: gender, year course was taken, term GPA, cumulative GPA, ACT score, and SAT score.

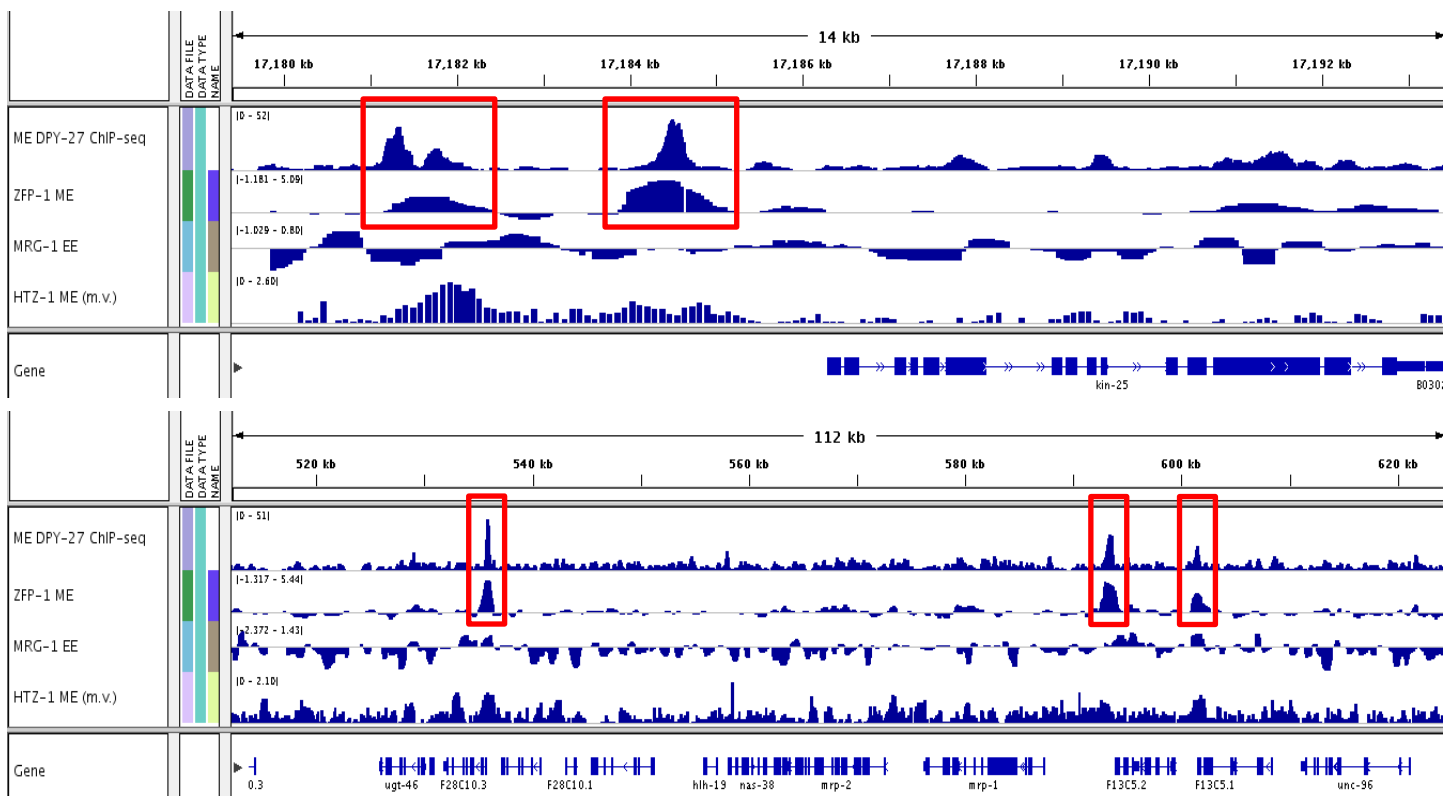
3 5 10 (uL; repeating)

rex-1 rex-2 rex-1 rex-2  
ChIP ChIP Input Input

myo-1(p) myo-1(e) myo-1(p) myo-1(e)  
ChIP ChIP Input Input

**Figure A1.11. DPY-27 Chromatin immunoprecipitation confirms prior occupancy results.** Shown is SDS-PAGE following PCR using pull-down DNA from DPY-27 ChIP from mixed stage WT embryos. Results mirror those seen in [8]. DPY-27 is present at *rex* sites and the *myo-1* promoter, but not an exonic *myo-1* region. All bands were 300-400bp, as expected.

A



B

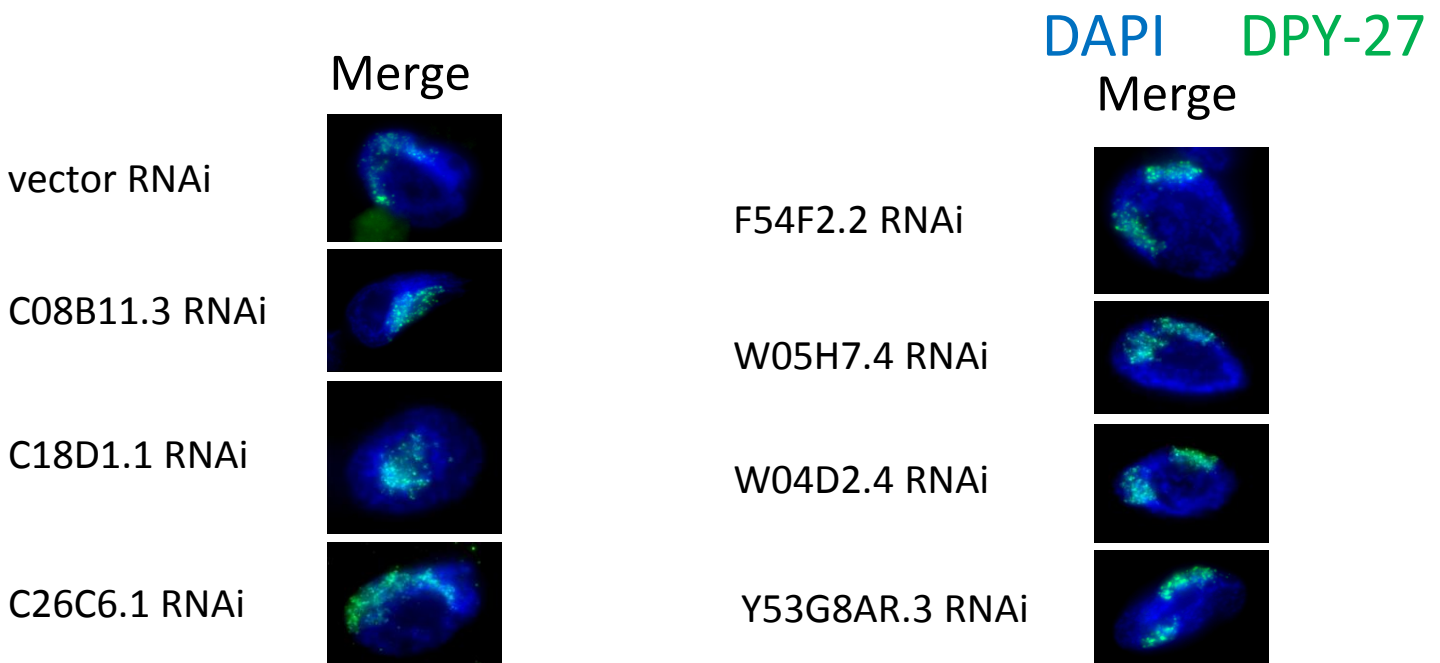


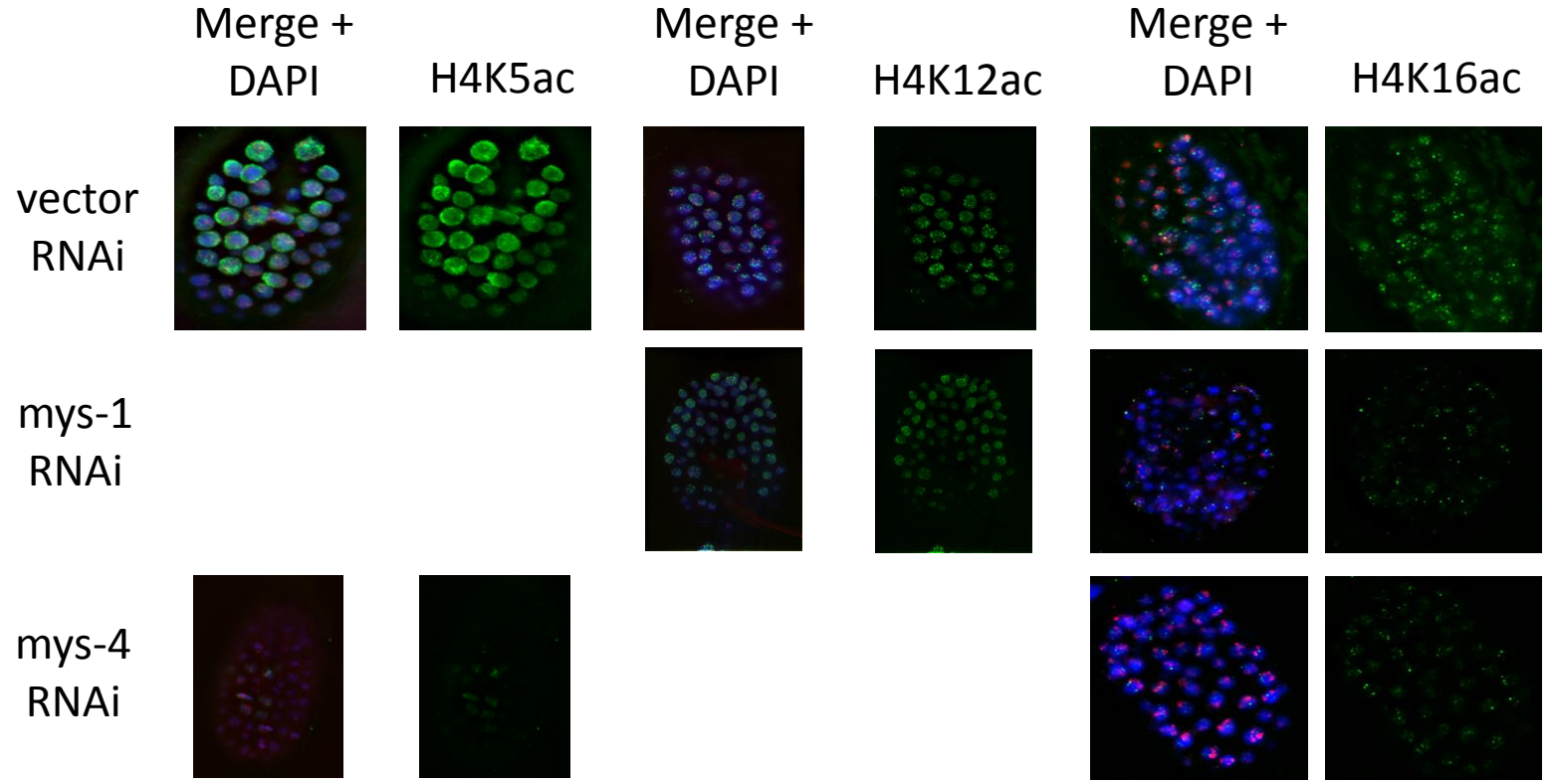
**Figure A1.12. A selection of zinc finger proteins do not contribute to DCC localization.** A) Browser window views taken in IGV showing mixed embryo DPY-27 ChIP-seq, ZFP-1, early embryo MRG-1 data, or mixed embryo HTZ-1 ChIP-chip data. Data show a distinct enrichment of ZFP-1 at DCC binding peaks. B) Immunofluorescence analysis of DPY-27 localization in WT worm gut nuclei following RNAi treatment against a variety of zinc finger proteins (either ZFP-1 or identified in DCC MuD-PIT analyses ([2,9]; unpublished results). Results indicate zinc finger protein gene knockdown did not cause DCC localization disruption.



A











RNAi against:	H4K5ac	H4K8ac	H4K12ac	H4K16ac
<i>mys-1</i>	NO	NO	YES	YES
<i>mys-2</i> ex. 1-3	NO	NO	NO	NO
<i>mys-2</i> ex. 5-7	NO	NO	NO	NO
<i>mys-3</i>	NO	NO	NO	NO
<i>mys-4</i>	YES	NO	NO	YES
<i>cbp-1</i>	NO	NO	NO	NO
<i>pcaf-1</i>	NO	NO	NO	NO
<i>tag-235</i> (e)	NO	NO	NO	NO
<i>tag-235</i> (gn)	NO	NO	NO	NO
<i>elpc-3</i>	NO	NO	NO	NO

B



**Figure A1.13. Identification of HAT proteins which acetylate histone H4 in *C. elegans*.** A) Summary table of HAT RNAi screen for changes in H4K5ac, H4K8ac, H4K12ac, or H4K16ac assayed by IF microscopy, with CAPG-1 antibody co-stain, in WT embryos and gut nuclei (negative data not shown). Results show that all acetylations could not be accounted for, but MYS-1 acetylates H4K12 and H4K16, and MYS-4 acetylates H4K5 and H4K16. B) IF images of ~200-500-cell embryos treated with vector or HAT protein RNAi showing positive results, reduced acetylation staining compared to vector RNAi levels. DAPI (DNA) is shown in blue.



Key		
	DC gene	
	nonDC gene	
	dox (active)	
	dox (poised)	
	dox (off)	
	rex (active)	
	rex (poised)	
	rex (off)	
	waystations (active)	
	waystations (poised)	

**Figure A1.14. An X chromosome feature distribution map.** Feature types shown were ordered in Microsoft Excel, corresponding boxes in the spreadsheet were color-coded, and the distribution was transferred. This distribution demonstrates clumps of *dox* and *rex* sites along X, and biases in overall distribution of X chromosome features. Chromosome start and end sites are labeled, but data do not follow a distance scale.

A

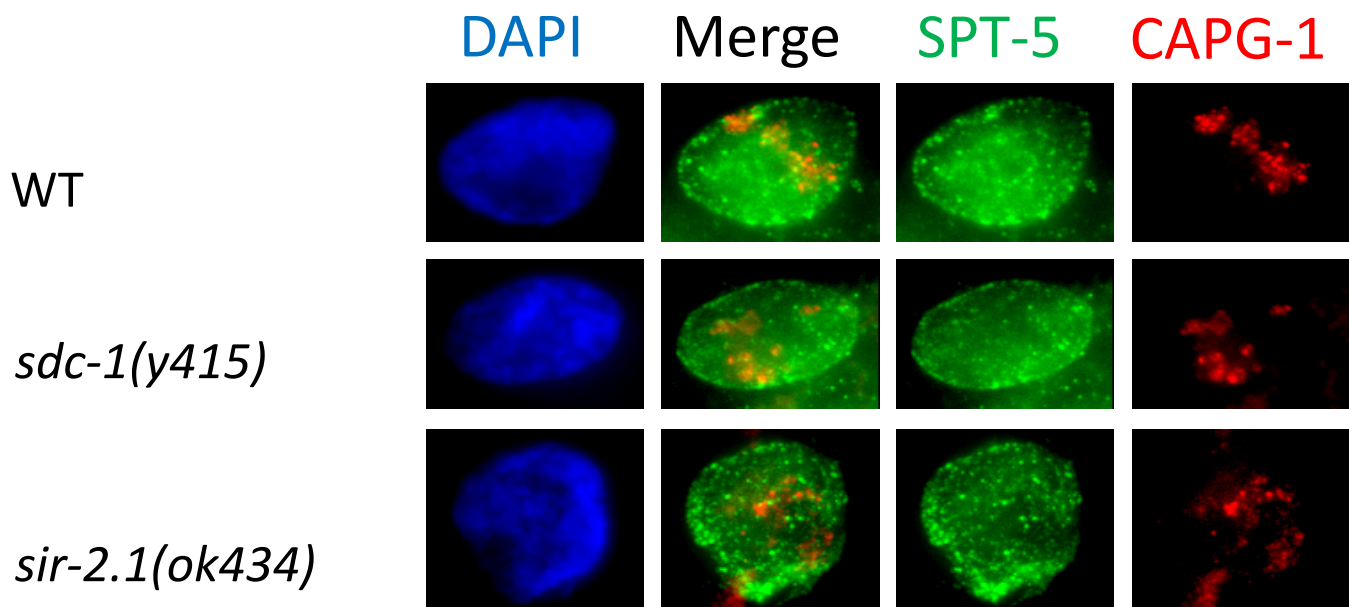
		Jans DC		Jans non-DC		MW DC		MW non-DC	
plus and minus tiRNAs		45	12.36%	28	9.76%	49	14.50%	24	10.81%
plus only or minus only tiRNA		147	40.38%	109	37.98%	136	40.24%	91	40.99%
plus strand only tiRNA		55	15.11%	36	12.54%	47	13.91%	35	15.77%
minus strand only tiRNA		92	25.27%	73	25.44%	89	26.33%	56	25.23%
All plus strand		100	27.47%	64	22.30%	96	28.40%	59	26.58%
All minus strand		137	37.64%	101	35.19%	138	40.83%	80	36.04%
Total # Genes in List		364		287		338		222	
4423 total	plus strand tiRNAs	17.64%	Average Autosomal frequency plus strand tiRNAs						
3900 autosomal	plus strand tiRNAs	11.82%	X chromosome frequency plus strand tiRNAs						
		16.67%	Expected chromosome frequency plus strand						
5848 total	minus strand tiRNAs	17.27%	Average Autosomal Frequency minus strand tiRNAs						
5049 autosomal	minus strand tiRNAs	13.66%	X chromosome frequency minus strand tiRNAs						
		16.67%	Expected chromosome frequency minus strand						

B

		Jans DC		Jans non-DC		MW DC		MW non-DC	
plus and minus tiRNAs		70	19.23%	44	15.33%	68	20.12%	44	19.82%
plus only or minus only tiRNA		155	42.58%	110	38.33%	147	43.49%	85	38.29%
plus strand only tiRNA		40	10.99%	40	13.94%	45	13.31%	35	15.77%
minus strand only tiRNA		115	31.59%	70	24.39%	102	30.18%	50	22.52%
All plus strand		110	30.22%	84	29.27%	113	33.43%	79	35.59%
All minus strand		185	50.82%	114	39.72%	170	50.30%	94	42.34%
Total # Genes in List		364		287		338		222	
4720 total	plus strand tiRNAs	23.66%	Autosomal Average frequency plus strand tiRNAs						
4056 A	plus strand tiRNAs	23.89%	X chromosome Average frequency plus strand tiRNAs						
		16.67%	Expected chromosome frequency plus strand						
6949 total	minus strand tiRNAs	34.76%	Average Autosomal Frequency minus strand tiRNAs						
5960 A	minus strand tiRNAs	35.59%	X chromosome frequency minus strand tiRNAs						
		16.67%	Expected chromosome frequency plus strand						

**Figure A1.15. tiRNA occurrence summary.** Using the small RNA-seq DataSet GSE11738, samples GSM297742 (mixed embryo; A) and GSM297745 (L3; B), 17nt RNA (tiRNAs [10-12]) abundances were calculated across dosage compensated or non-dosage compensated genes {both sets of lists, [13] and MW unpublished (see Chapter 3)}. Results show that tiRNA abundance increased when comparing embryo to L3 data, suggesting that tiRNA abundance is not directly correlated with dosage compensation activity. Bioinformatics assistance was obtained from Rich McEachin (Department of Computational Medicine & Bioinformatics).

A



B

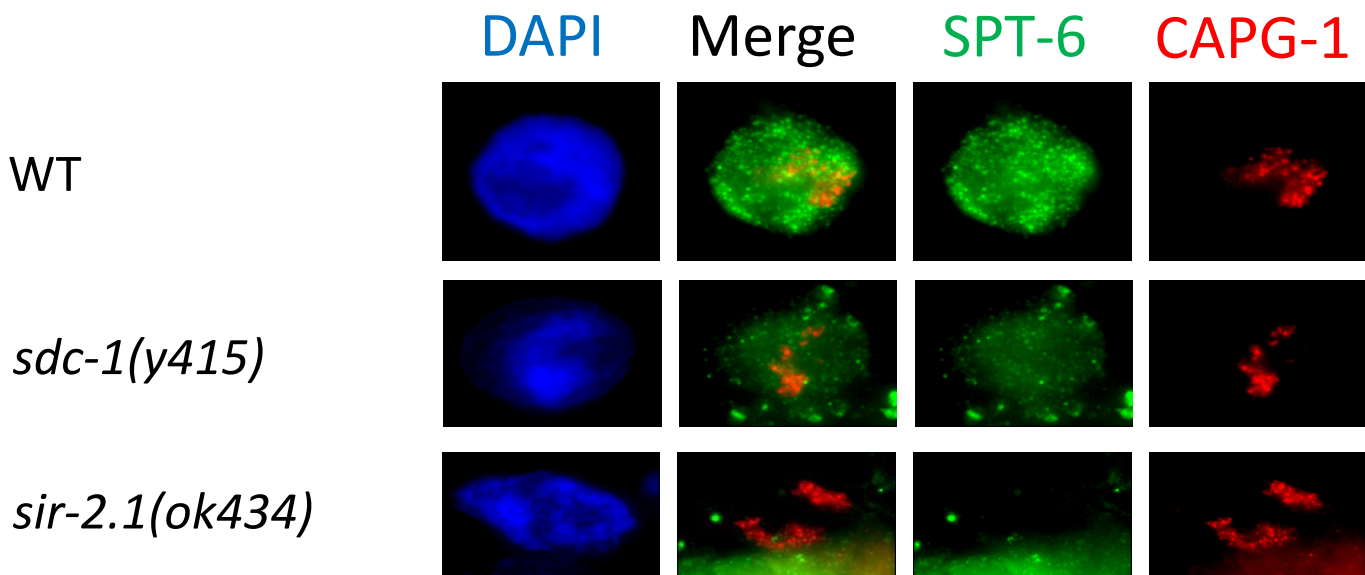
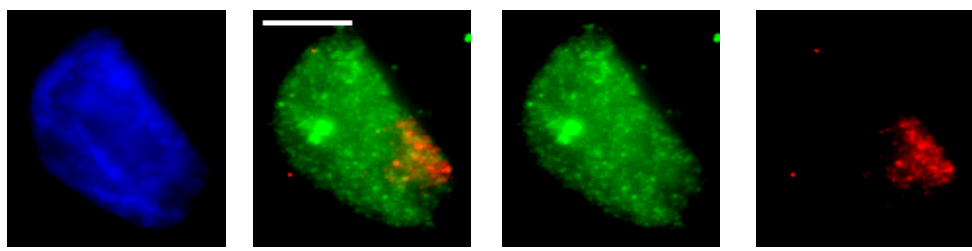


**Figure A1.16. Evaluation of SPT-5 and SPT-6 localization dependence on dosage compensation and SIR-2.1 function.** Shown are hermaphrodite gut nuclei stained with: (A) SPT-5 and CAPG-1 antibodies, or (B) SPT-6 and CAPG-1 antibodies from WT, *sdc-1(y415)*, or *sir-2.1(ok434)* worms. DAPI (DNA) is shown in blue. In these mutants SPT-5 accumulates around the nuclear periphery, while SPT-6 shows a reliance on both SDC-1 and SIR-2.1 for proper expression or stability. Staining from both antibodies were specific, as signal disappeared from the nucleus after RNAi against the antibody target locus, *spt-5* or *spt-6* (data not shown).

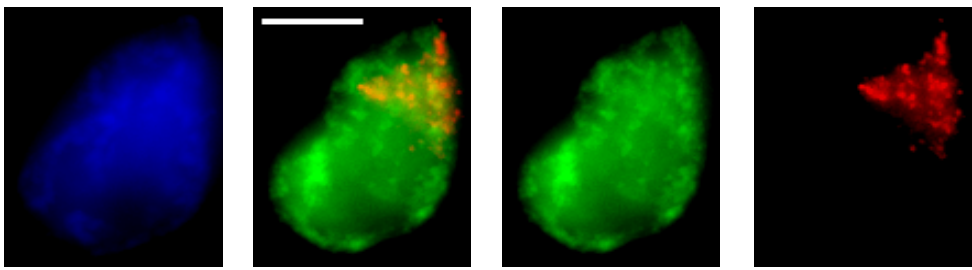
A

DAPI Merge SIR-2.1 CAPG-1

WT



*dpy-21 (e428)*



B

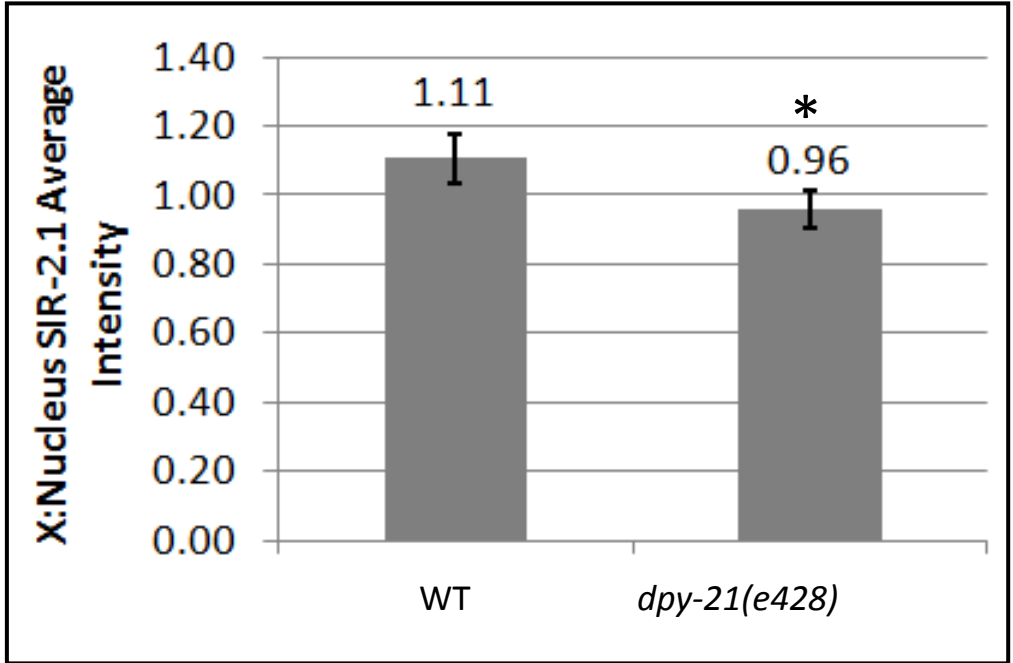


**Figure A1.17. A slight SIR-2.1 enrichment on X depends on DPY-21.** Shown are hermaphrodite gut nuclei from WT or *dpy-21(e428)* stained with SIR-2.1 and CAPG-1 antibodies (A). DAPI (DNA) is shown in blue. (B) Graph of fluorescence intensity quantification of (A). Results show a small, but reproducible, enrichment of SIR-2.1 signal in WT gut nuclei, that is abolished in *sir-2.1(ok434)*. Asterisk indicates a significant difference ( $p < 0.05$ ) difference between WT and *sir-2.1(ok434)* conditions.

PAS sequences	# of occurrences		
Sequence	DC genes	nonDC genes	DCC components
AATAAT	14	7	1
ATTAAA	26	15	5
AATAAA	265	180	4
AATGAA	61	64	7
GGTAAA	2	4	1
CATAAA	29	18	2
AATGTA	15	9	1
TATGAA	26	11	0
AAAACA	7	3	0
AATTAA	4	3	0
GATAAA	27	12	0
AGTAAA	13	14	0
TTTAAA	9	9	0
TATAAA	44	35	3
AATATA	9	5	1
CAAAAA	4	3	0
TCTAAA	14	5	0
AAAAAA	13	12	0
AATACA	16	8	1
CATGAA	7	5	0
GATGAA	5	6	0
AATAAG	6	1	0
TGTAAA	7	3	0
ACTAAA	5	3	1
AATTAAA	1	0	0
No 3'UTR found	0	21	0
No signal	150	88	7
Total	629	435	27
Total PAS excluding AATAAA	364	255	23

**Figure A1.18. Polyadenylation sequence usage analysis reveals greater variety and occurrence of PAS usage.** Performed by Anna Cacciaglia. Data for 3' UTR PAS usage for dosage compensated, non-dosage compensated (both from Jans et al., 2009 lists), or DCC components were collected manually using 3' UTRome (<http://asparagus.bio.nyu.edu/cgi-bin/UTRome/utrome.cgi?action=search>). Results show that dosage compensated genes show a greater variety and abundance of PAS usage than non-dosage compensated genes.

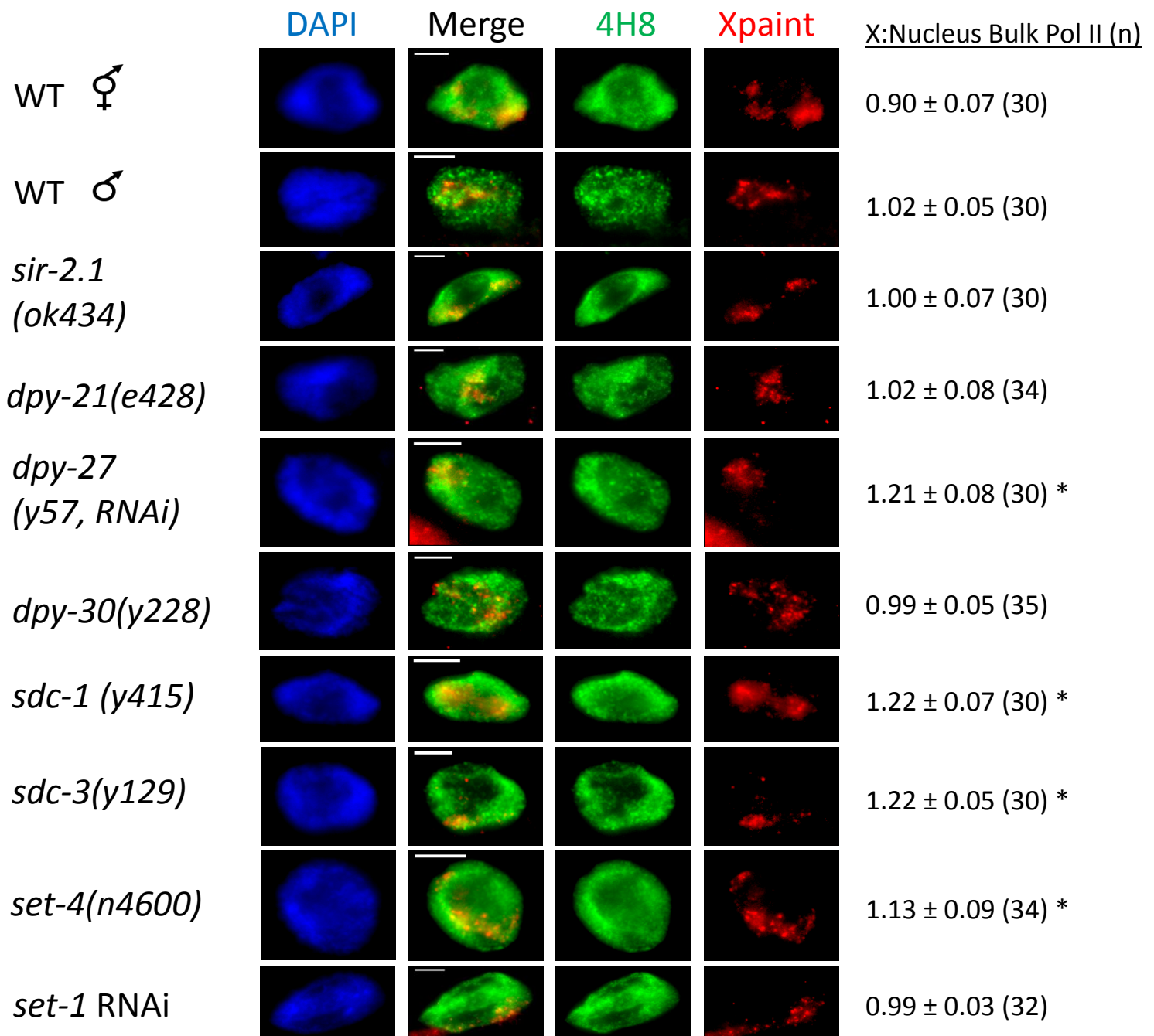


**Figure A1.19. Dependence of hypo-phosphorylated RNA Pol II localization on dosage compensation.** Shown are gut nuclei from hermaphrodite or male worms of various mutant backgrounds stained with antibodies against hypo-phosphorylated RNA Pol II (4H8) and CAPG-1. DAPI (DNA) is shown in blue. Scale bars are 5 microns in length. Results show no enrichment of 4H8 on X in WT hermaphrodite or male nuclei, but a significant enrichment on X in several dosage compensation mutants and *set-4*(*n4600*).

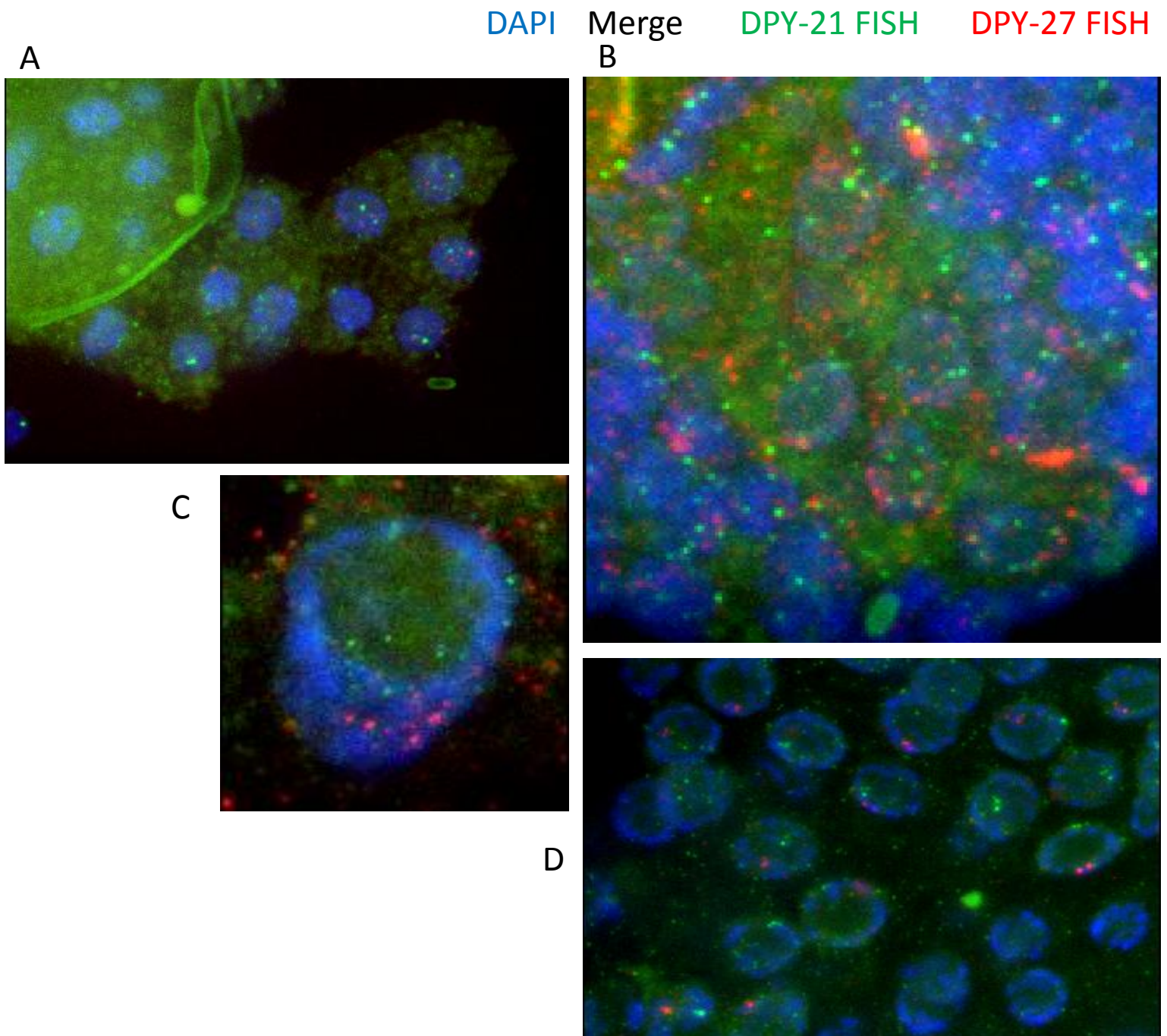


**Figure A1.20. Timing comparison of DPY-21 and DPY-27 expression.** Shown are various cell/tissue types from WT hermaphrodites treated with fluorescent *in situ* hybridization probes against portions of *dpy-21* or *dpy-27* transcripts. DAPI (DNA) is shown in blue. Panels are as follows: A) 30-cell embryo. B) ~200-cell embryo. C) gut nucleus. D) germline. Results show robust signal from DPY-21 transcripts throughout all tissues analyzed, whereas significant signal in addition to the native loci was only seen from DPY-27 FISH in mid-late embryos (B).



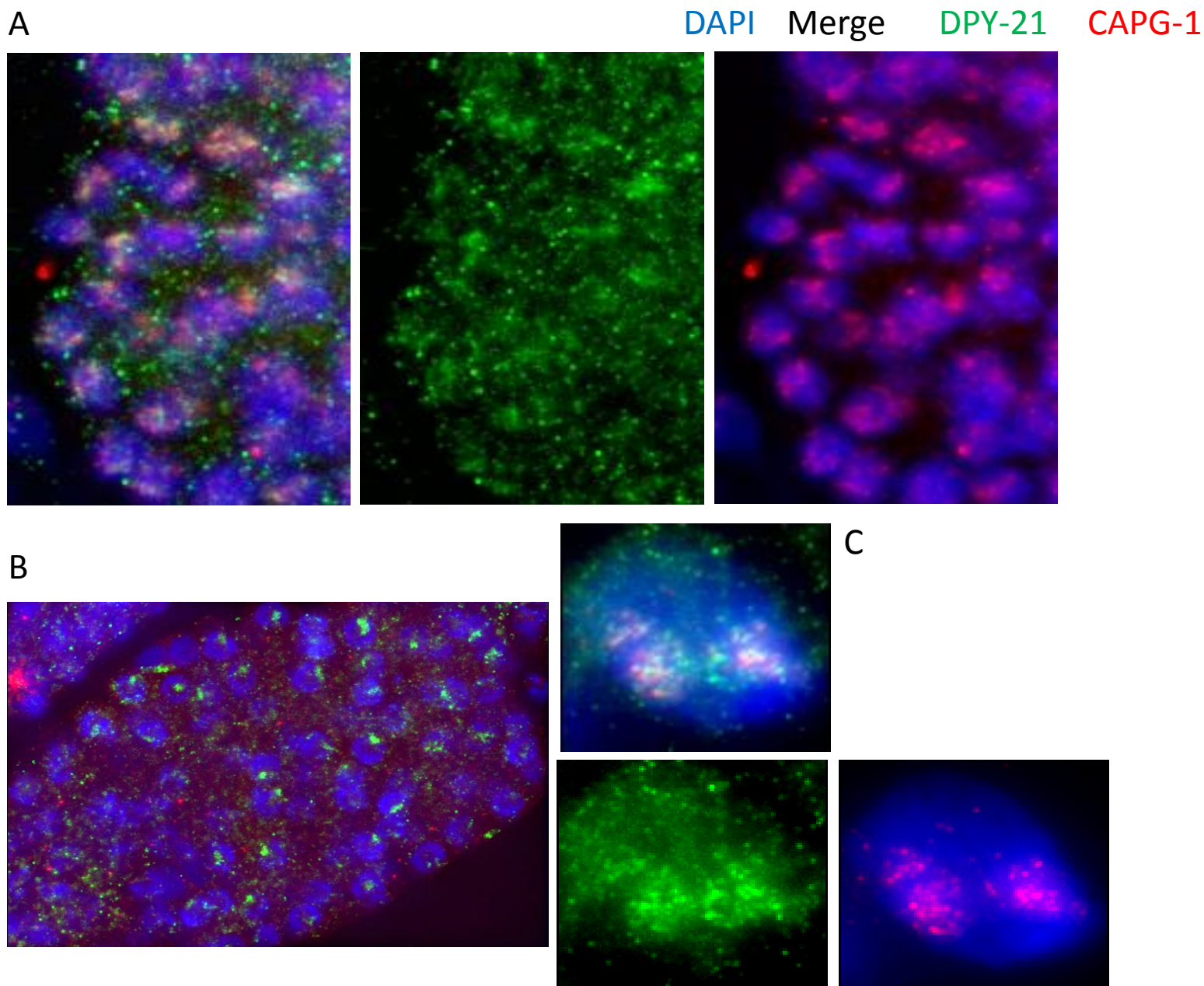


**Figure A1.21. DPY-21 Localization in various tissue types from WT worms.** Performed by Anna Cacciaglia. Shown are: A) embryonic nuclei, B) germline, and C) gut nucleus images from WT worms stained with antibodies against DPY-21 and CAPG-1. DAPI (DNA) is shown in blue. Results dispute published data [14], which suggest DPY-21 localization is mainly confined to X. Our results show that DPY-21 signal is indeed most robust on X, but that a good deal of verifiable signal (Compare to Figure A1.22) is present on autosomes. Further, clear signal is seen concentrated in a region between chromosomes in germline nuclei, which is not the case for other DCC components.

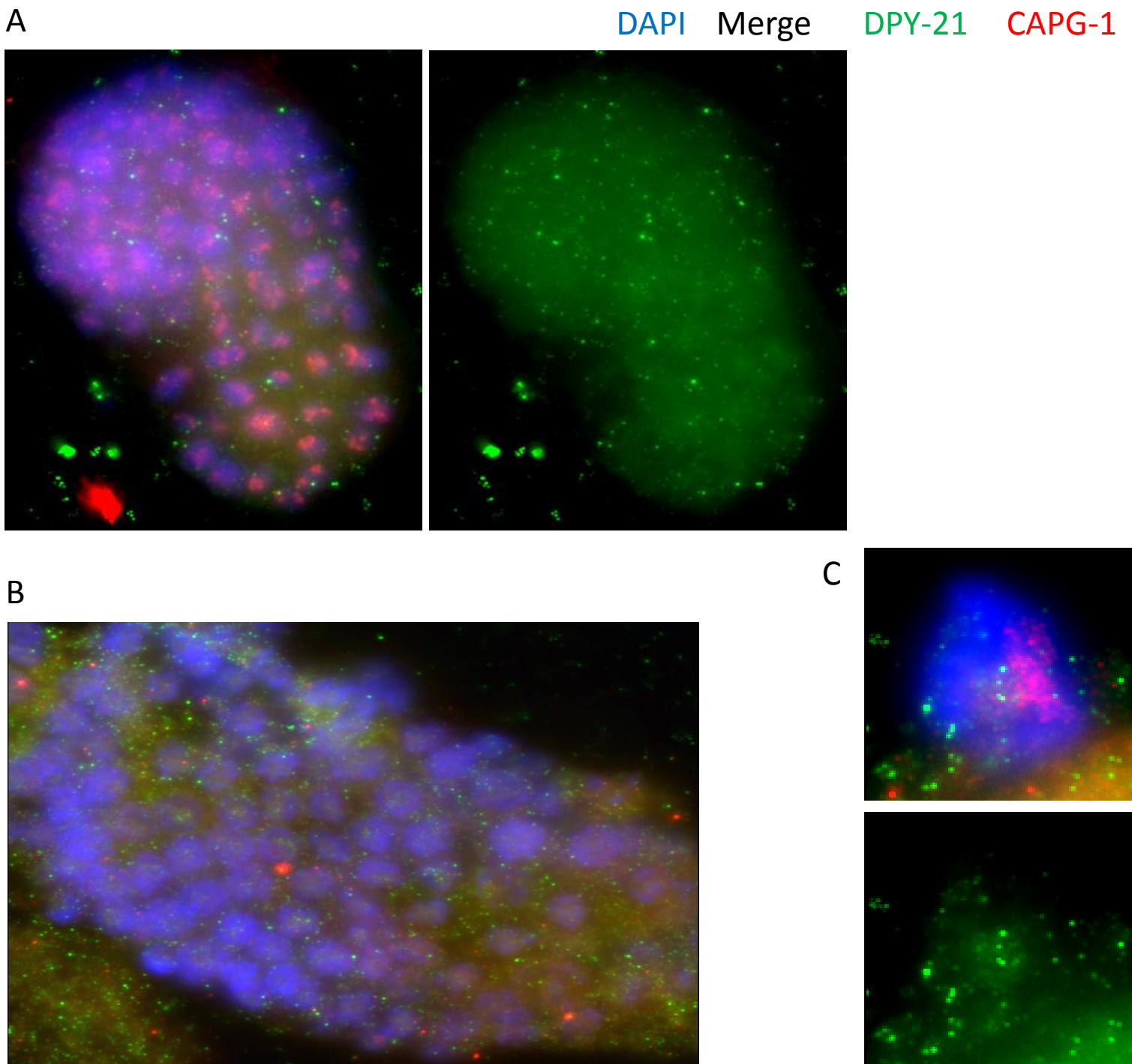


**Figure A1.22. The DPY-21 antibody staining patterns are specific for DPY-21.** Performed by Anna Cacciaglia. Shown are: A) embryonic nuclei, B) germline, and C) gut nucleus images from *dpy-21(e428)* worms stained with DPY-21 and CAPG-1 antibodies. DAPI (DNA) is shown in blue. Results show a loss of all specific staining in this mutant background (as compared to Figure A1.21).

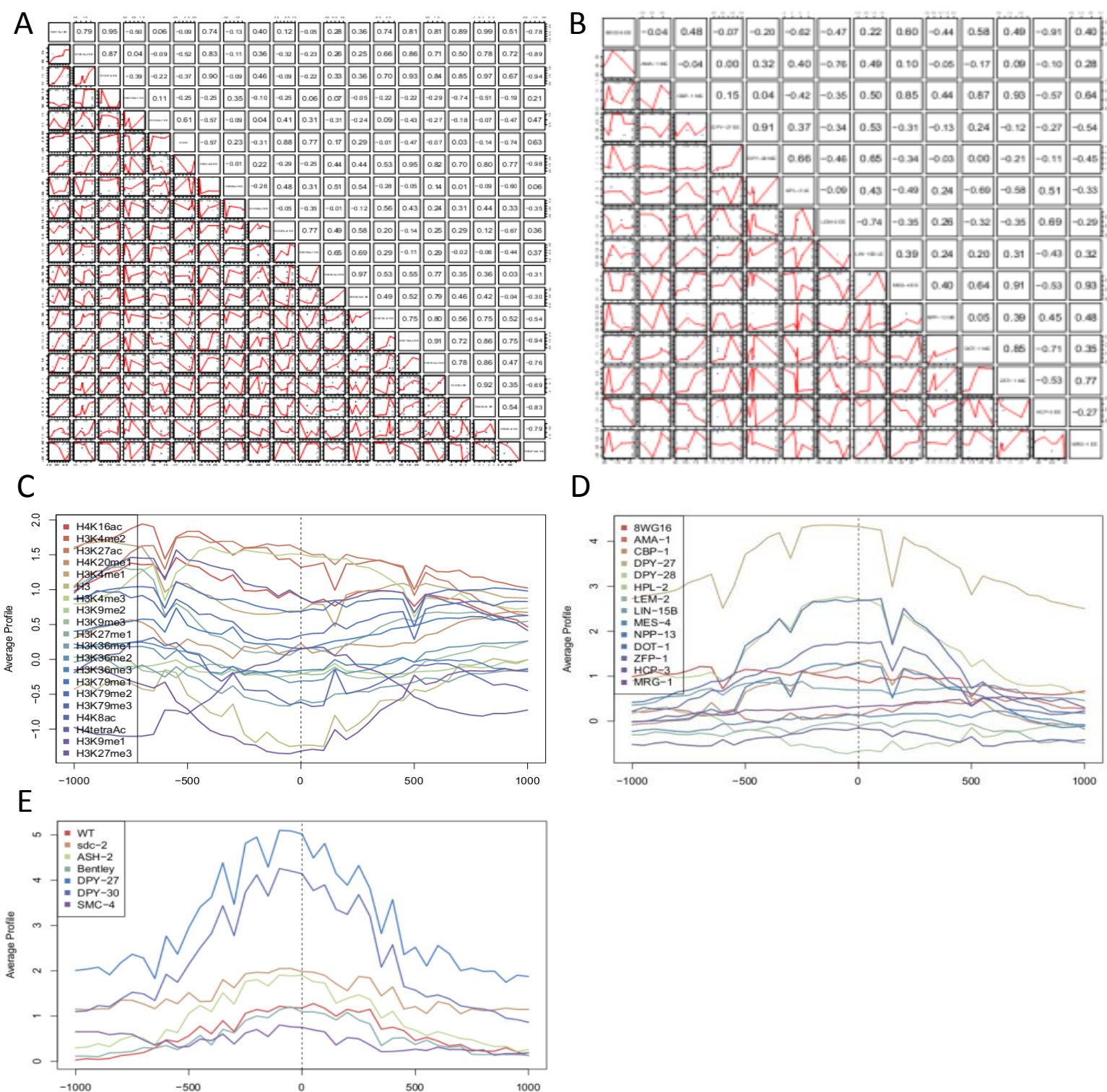


**Figure A1.23. Histone modification and protein occupancy over all active enhancer-type rex sites.** Shown are cross-correlation tables (A & B) or SitePro feature-centered meta-analysis (C-E) displaying histone modification (modENCODE; A, C), transcription factor (modENCODE; B, D), or COMPASS/DCC ([15]; E) occupancy over all active enhancer-type (bimodal H3K4me1 signal) rex sites. Results show peaks in protein occupancy, while many histone modifications peak upstream and steadily decline over these sites.

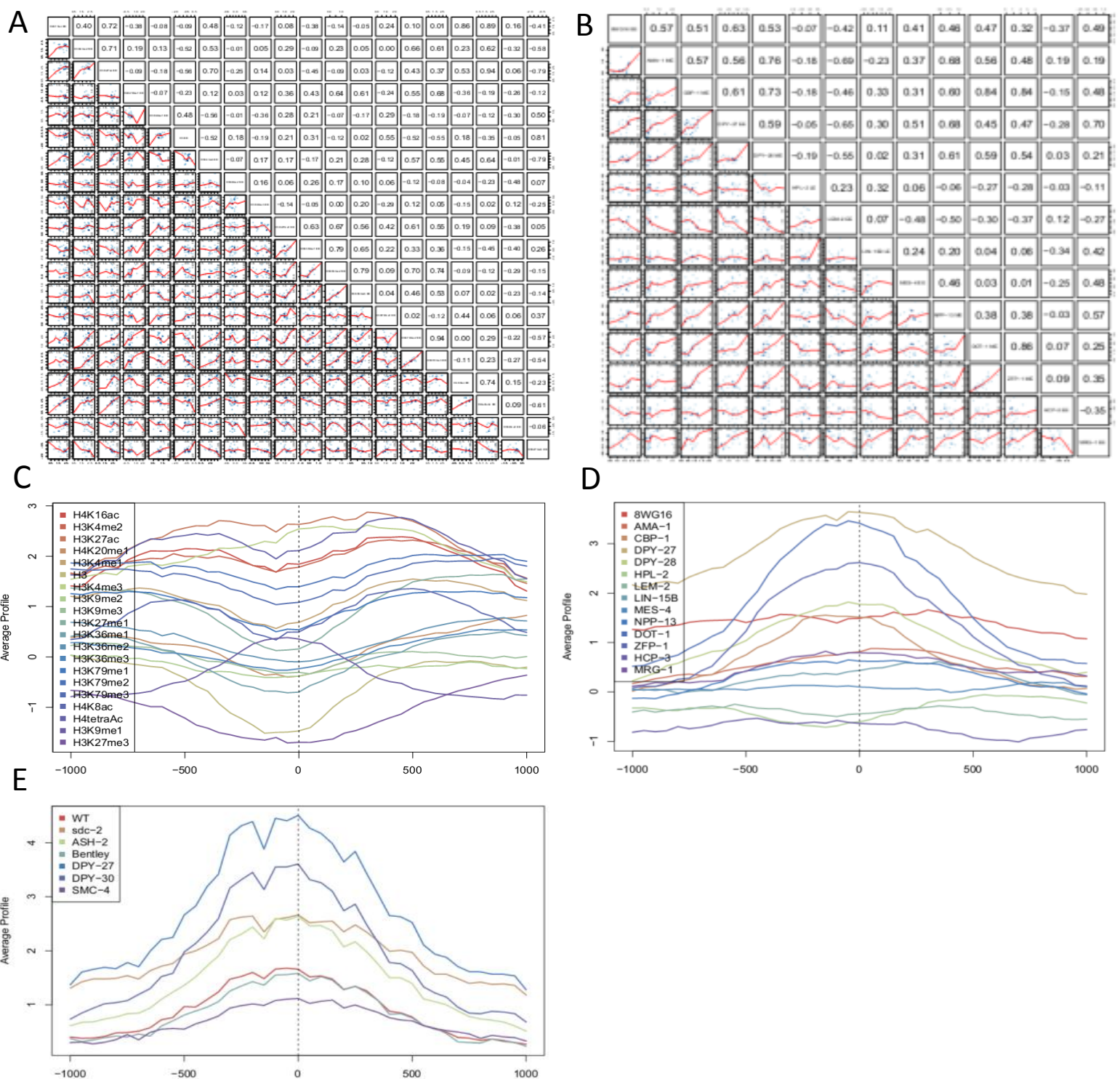


**Figure A1.24. Histone modification and transcription factor occupancy over all active enhancer-type dox sites.** Shown are cross-correlation tables (A & B) or SitePro feature-centered meta-analysis (C-E) displaying histone modification (modENCODE; A, C), transcription factor (modENCODE; B, D), or COMPASS/DCC ([15]; E) occupancy over all active enhancer-type (bimodal H3K4me1 signal) dox sites. Results show peaks or valleys in histone modification and protein occupancy centered over these sites.

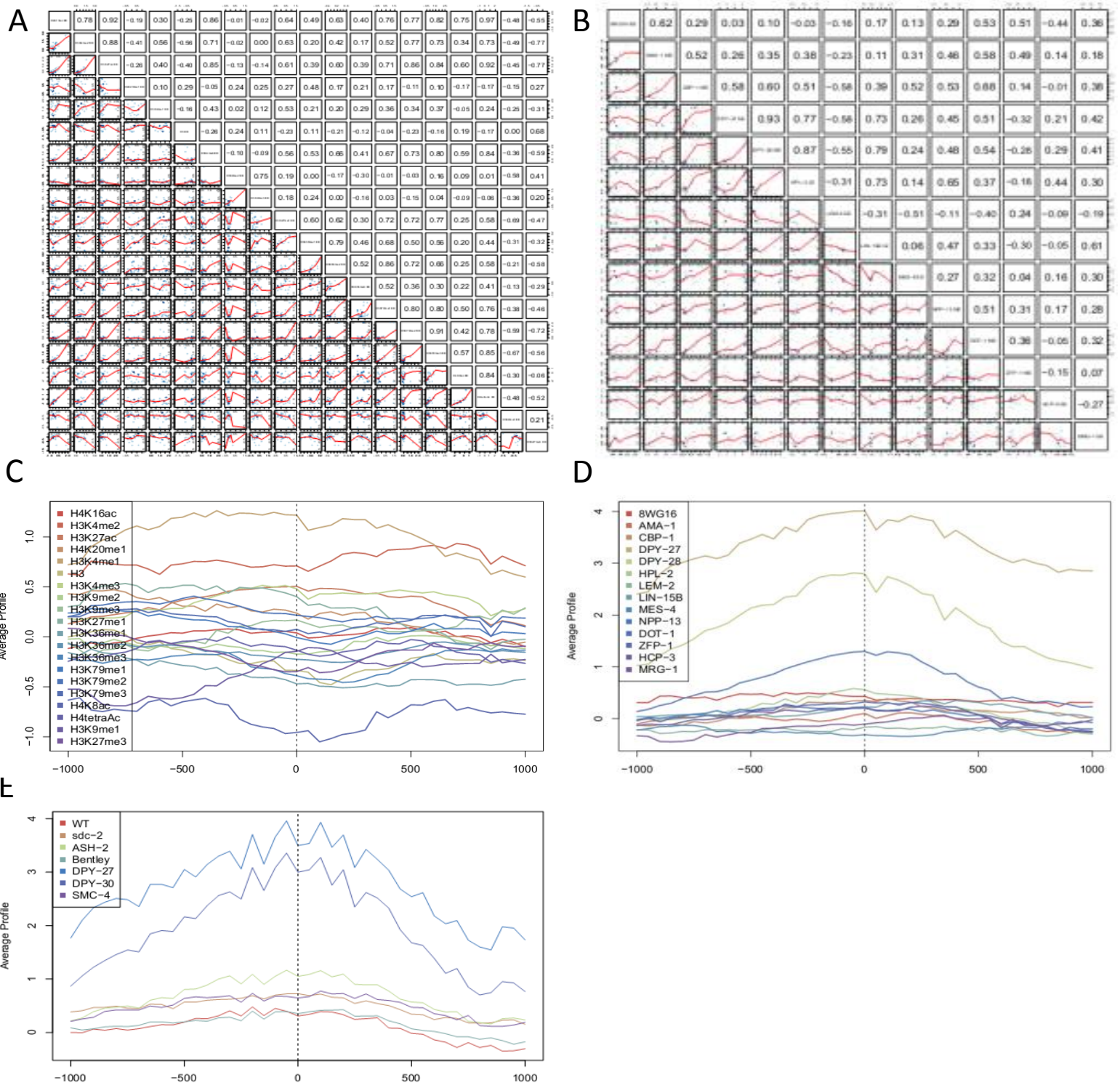


**Figure A1.25. Histone modification and transcription factor occupancy over all poised enhancer-type rex sites.** Shown are cross-correlation tables (A & B) or SitePro feature-centered meta-analysis (C-E) displaying histone modification (modENCODE; A, C), transcription factor (modENCODE; B, D), or COMPASS/DCC ([15]; E) occupancy over all poised enhancer-type (monomodal H3K4me1 signal) rex sites. Results show broad peaks or low flat signal profiles in histone modification and protein occupancy centered over these sites.

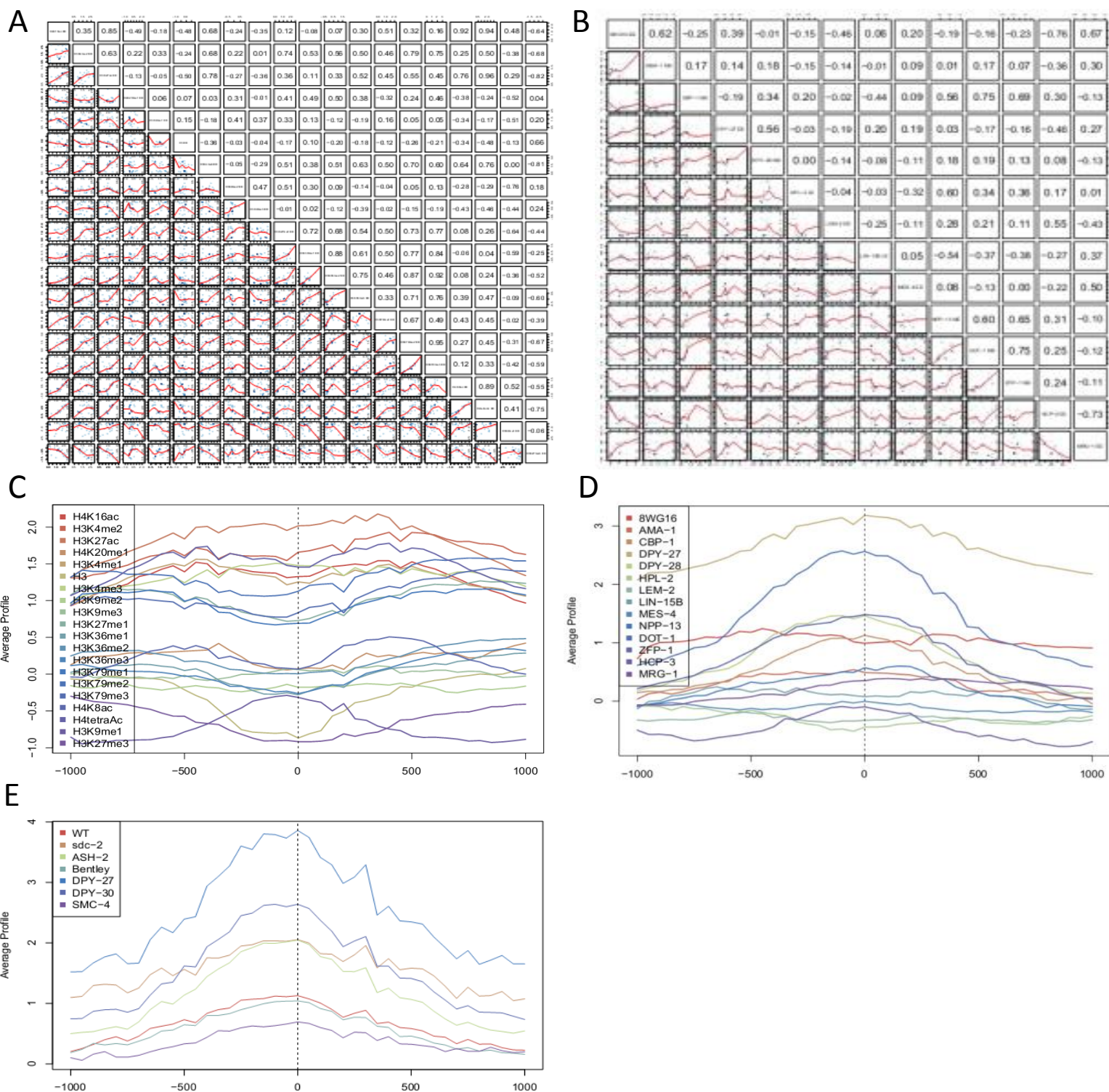


**Figure A1.26. Histone modification and transcription factor occupancy over all poised enhancer-type dox sites.** Shown are cross-correlation tables (A & B) or SitePro feature-centered meta-analysis (C-E) displaying histone modification (modENCODE; A, C), transcription factor (modENCODE; B, D), or COMPASS/DCC ([15]; E) occupancy over all poised enhancer-type (monomodal H3K4me1 signal) dox sites. Results show peaks and valleys in histone modification and protein occupancy centered over these sites.

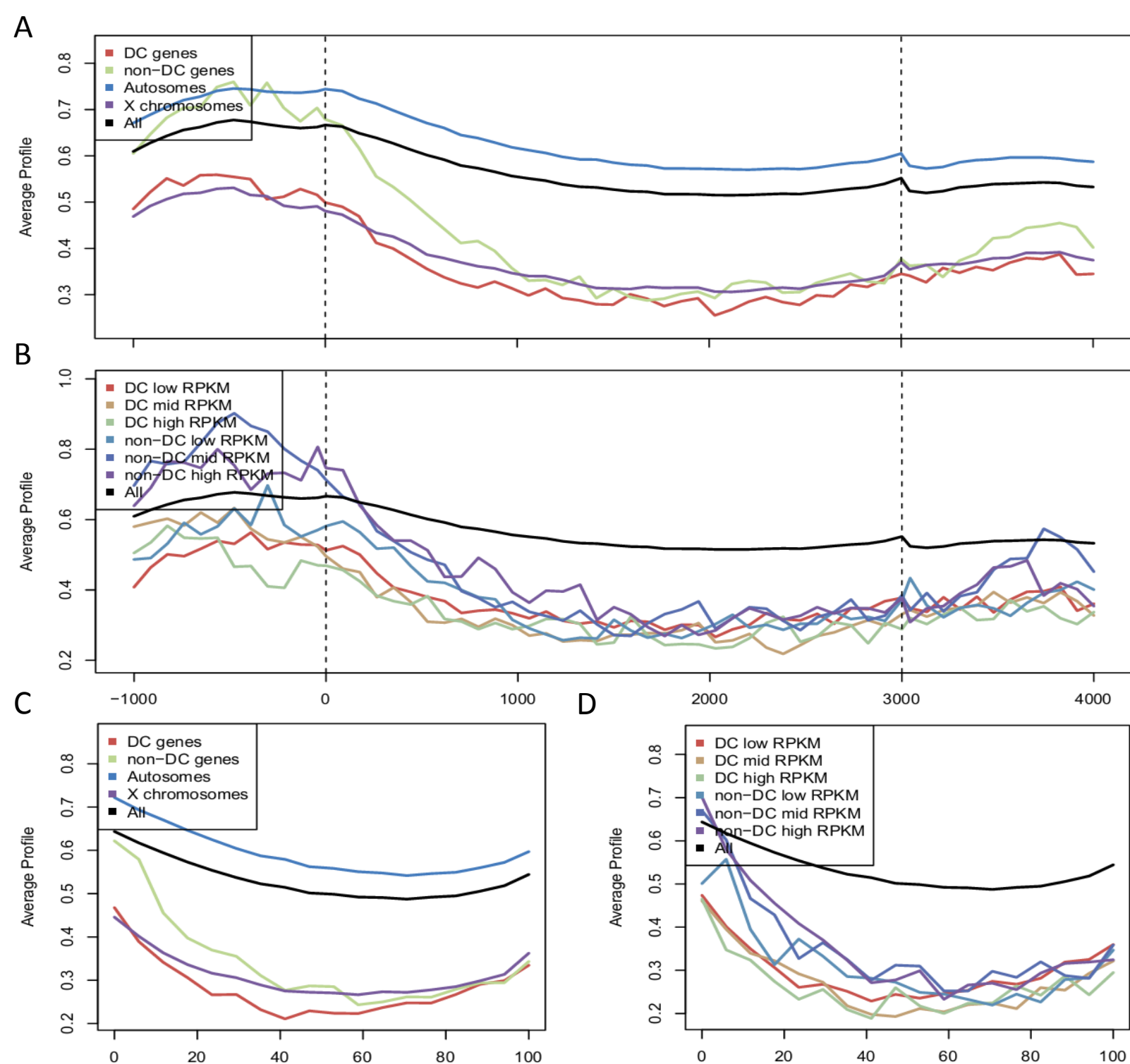


**Figure A1.27. HTZ-1 gene group and transcription level metagene analysis.** Shown are metagene profiles (A & B) or concatenated exon profiles (C & D) comparing dosage compensated, non-dosage compensated, active X, and active autosome (A & C) or low, medium, and highly transcribed dosage compensated or non-dosage compensated (B & D) gene HTZ-1 occupancy in WT mixed stage embryos. Results show  $\sim 1.5$ -fold lower levels of HTZ-1 at dosage compensated genes than non-dosage compensated genes and autosomes compared to X. This difference is not well correlated with degree of transcription of each gene set, but levels are lower, if anything, at higher transcribed genes.

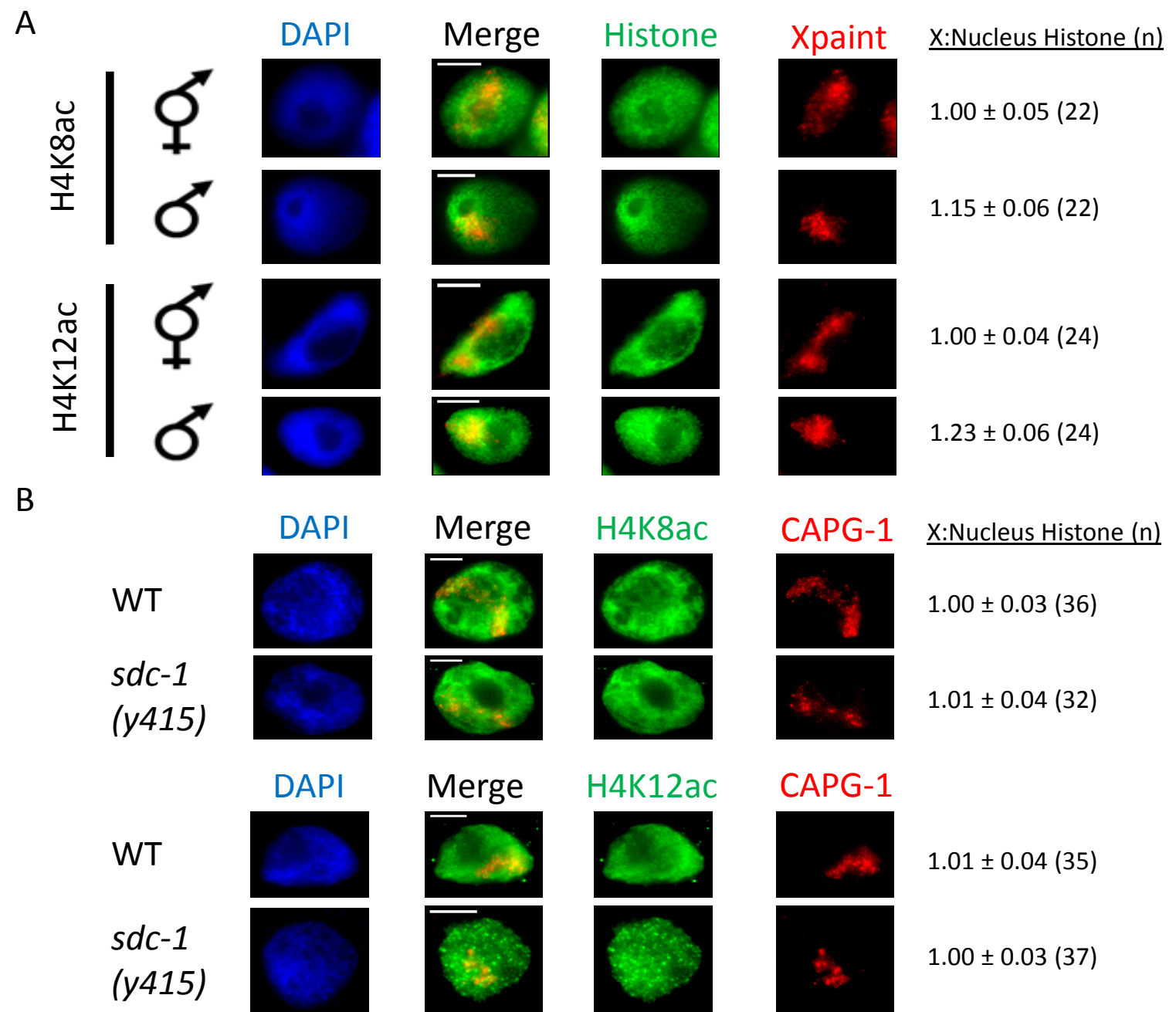


**Figure A1.28. H4K8ac and H4K12ac enrichment on male X chromosomes.** Shown are representative IF images from WT males or hermaphrodites treated with Xpaint FISH and antibodies to histone modifications (A) or antibodies against histone modifications and CAPG-1 (B). DAPI (DNA) is shown in blue. Slides for (A) made by Martha Snyder. Results show enrichment of H4K8ac and H4K12ac on male X chromosomes (A), that is not seen in hermaphrodites and is not the result of a DCC-dependent decrease on hermaphrodite X chromosomes (B).



## References

1. Wells MB, Snyder MJ, Custer LM, Csankovszki G (2012) *Caenorhabditis elegans* dosage compensation regulates histone H4 chromatin state on X chromosomes. *Mol Cell Biol* 32: 1710-1719.
2. Csankovszki G, Collette K, Spahl K, Carey J, Snyder M, et al. (2009) Three distinct condensin complexes control *C. elegans* chromosome dynamics. *Curr Biol* 19: 9-19.
3. Ercan S, Dick LL, Lieb JD (2009) The *C. elegans* dosage compensation complex propagates dynamically and independently of X chromosome sequence. *Curr Biol* 19: 1777-1787.
4. Baugh LR, Demodena J, Sternberg PW (2009) RNA Pol II accumulates at promoters of growth genes during developmental arrest. *Science* 324: 92-94.
5. Lian Z, Karpikov A, Lian J, Mahajan MC, Hartman S, et al. (2008) A genomic analysis of RNA polymerase II modification and chromatin architecture related to 3' end RNA polyadenylation. *Genome Res* 18: 1224-1237.
6. Xie SQ, Martin S, Guillot PV, Bentley DL, Pombo A (2006) Splicing speckles are not reservoirs of RNA polymerase II, but contain an inactive form, phosphorylated on serine2 residues of the C-terminal domain. *Mol Biol Cell* 17: 1723-1733.
7. Alcover A, Izquierdo M, Stollar D, Kitagawa Y, Miranda M, et al. (1982) In situ immunofluorescent visualization of chromosomal transcripts in polytene chromosomes. *Chromosoma* 87: 263-277.
8. Blauwkamp TA, Csankovszki G (2009) Two classes of dosage compensation complex binding elements along *Caenorhabditis elegans* X chromosomes. *Mol Cell Biol* 29: 2023-2031.
9. Petty EL, Collette KS, Cohen AJ, Snyder MJ, Csankovszki G (2009) Restricting dosage compensation complex binding to the X chromosomes by H2A.Z/HTZ-1. *PLoS Genet* 5: e1000699.
10. Taft RJ, Kaplan CD, Simons C, Mattick JS (2009) Evolution, biogenesis and function of promoter-associated RNAs. *Cell Cycle* 8: 2332-2338.
11. Taft RJ, Simons C, Nahkuri S, Oey H, Korbie DJ, et al. (2010) Nuclear-localized tiny RNAs are associated with transcription initiation and splice sites in metazoans. *Nat Struct Mol Biol* 17: 1030-1034.
12. Taft RJ, Glazov EA, Cloonan N, Simons C, Stephen S, et al. (2009) Tiny RNAs associated with transcription start sites in animals. *Nat Genet* 41: 572-578.
13. Jans J, Gladden JM, Ralston EJ, Pickle CS, Michel AH, et al. (2009) A condensin-like dosage compensation complex acts at a distance to control expression throughout the genome. *Genes Dev* 23: 602-618.
14. Yonker SA, Meyer BJ (2003) Recruitment of *C. elegans* dosage compensation proteins for gene-specific versus chromosome-wide repression. *Development* 130: 6519-6532.
15. Pferdehirt RR, Kruesi WS, Meyer BJ (2011) An MLL/COMPASS subunit functions in the *C. elegans* dosage compensation complex to target X chromosomes for transcriptional regulation of gene expression. *Genes Dev* 25: 499-515.